

**A STUDY OF THE EFFECTS OF VARIOUS FLOW OBSTRUCTIONS ON  
HETEROGENEOUS MICROMIXING IN BIOCATALYTIC  
MICROCHANNELS**

By  
Stephanie Wilson

Departmental Honors Thesis  
The University of Tennessee at Chattanooga  
Chemical Engineering

Project Director: Dr. Frank Jones  
Examination Date: 10/20/2006

Dr. Jim Henry  
Dr. Jim Hiestand  
Dr. Cecelia Wigal  
Dr. Neslihan Alp

Examining Committee Signatures:

---

Project Director

---

Department Examiner

---

Department Examiner

---

Department Examiner

---

Department Examiner

---

Liaison, Departmental Honors Committee

---

Chairperson, University Departmental Honors Committee

<b>ABSTRACT</b>	<b>III</b>
<b>INTRODUCTION</b>	<b>1</b>
<b>BACKGROUND</b>	<b>4</b>
MICROREACTOR FABRICATION	5
PDMS-E BIOPLASTIC REACTOR	6
EXPERIMENTAL RESULTS FROM SUPPORTING LITERATURE	7
<b>SUPPORTING THEORY</b>	<b>8</b>
GOVERNING EQUATIONS	9
BOUNDARY CONDITIONS	11
DIMENSIONLESS PARAMETER	11
NUMERICAL SOLUTIONS METHOD	12
<b>DESIGN SIMULATION DETAILS</b>	<b>13</b>
<b>RESULTS AND DISCUSSION</b>	<b>18</b>
EFFECT OF DESIGN ON FLUID REDISTRIBUTION	19
<i>EMPTY CHANNEL</i>	19
<i>ONE TRIANGLE CONFIGURATION</i>	22
<i>TWO TRIANGLE INLINE CONFIGURATION</i>	25
<i>TWO TRIANGLE ASYMMETRIC CONFIGURATION</i>	27
<i>THREE TRIANGLE CONFIGURATION</i>	29
EFFECT OF DESIGN ON CONVERSION	30
EFFECT OF TRIANGLE POSITION ON FLUID REDISTRIBUTION	36
<i>TWO TRIANGLE ASYMMETRIC 2/5 CONFIGURATION</i>	36
<i>TWO TRIANGLE ASYMMETRIC 1/3 CONFIGURATION</i>	37
EFFECT OF TRIANGLE POSITION ON CONVERSION	39
THE EFFECT OF DESIGN ON PRESSURE DROP	43
EFFECT OF DESIGN ON SHEAR STRESS AT THE WALLS	45
<b>CONCLUSIONS</b>	<b>46</b>
<b>REFERENCES</b>	<b>48</b>
<b>APPENDIX</b>	<b>50</b>

## Abstract

The results of a numerical study of the fundamental interactions of engineering design and micromixing on conversion in packed microchannels are presented. Previously, channel-based microreactors made of molded silicon plastic were designed, fabricated, and experimentally tested. These reactors have enzymes immobilized on the channel walls by various methods. They also contain molded packing particles to add reactive surface area and to redistribute the fluid. An intuitive packing arrangement was used in experimental studies and modeled successfully by computer simulation.

A computer simulation study was conducted to understand how changes in packing arrangement and number of packing particles affect micromixing and conversion efficiency. The experimental reactors were simulated using CFD-ACE+ multiphysics software. The focus of this study is to optimize the placement and number of packing to more efficiently meet conversion goals, taking into account micro fabrication and operational constraints. Microfluidic fundamentals such as Reynolds number ( $Re$ ), shear stress, and pressure drop are also explored due to variations in design features. The micro scale dimensions of the channel cross section (125 by 500 micrometers) cause all flows to be laminar. Behavior in the range  $0.1 < Re < 100$  is examined.

## Introduction

The fields of chemical engineering and nanotechnology have in recent times overlapped, creating the rapidly growing field of chemical process miniaturization. The microreactor is the progeny of this merger and promises improvements in chemical process control, product quality, and safety. Typically, a microreactor consists of any number of micro-sized pipes or channels through which fluid passes and undergoes a chemical reaction. On the order of tens to hundreds of micrometers in size, the very small cross-dimensions of these channels offer large surface area to volume ratios allowing for rapid heat and mass transfer. This small scale also creates a more efficient use of reactive sites, improving yield and selectivity. As with industrial scale reactors, the performance of a microreactor is improved by the addition of packing particles. These packing particles serve to redistribute the reacting fluid. Applicable to biological processes as well, the microreactor is renamed “biomicroreactor” when all inside surfaces of the channels, including packing, are coated with an enzyme to mimic a biological system and its corresponding reactions. In the biomicroreactor system, heterogeneous catalysis occurs when fluid reacts with the solid enzyme active surfaces.

The small size and resulting large surface area to volume ratios of microreactors make them more sensitive to slight changes in design. Changes in the number of packing particles, their shapes, and their locations within the channels may improve the reactor effectiveness significantly. Presently, the optimization of such

designs is a major concern in the fields that employ micro/nano technology. Design improvements are necessary to increase the reactor's ability to create product efficiently and affordably. However, fabrication and physical experimentation is a long and expensive process. Enzymes alone can cost well over \$2,000 per oz (cost of catalase). Additionally, thousands of experiments could be run to optimize packing design. Since physical experiments are expensive and time consuming, computer simulation is preferred.

The present study uses Computational Fluid Dynamics (CFD) software to model a catalase bioreactor in lieu of physical experiments. Validation of this technique comes from past successful CFD modeling of physical experimentation with a similar urease bioreactor [1, 3]. Figure 1 shows a Scanning Electron Micrograph of the physical  $500\mu\text{m} \times 125\mu\text{m} \times 500\text{mm}$  urease bioreactor channel with an intuitive but arbitrarily chosen packing configuration. Figure 2 shows a portion of the grid created for CFD simulation of the channel.



**Figure 1. SEM of Microchannel Used in Physical Experimentation [1]**

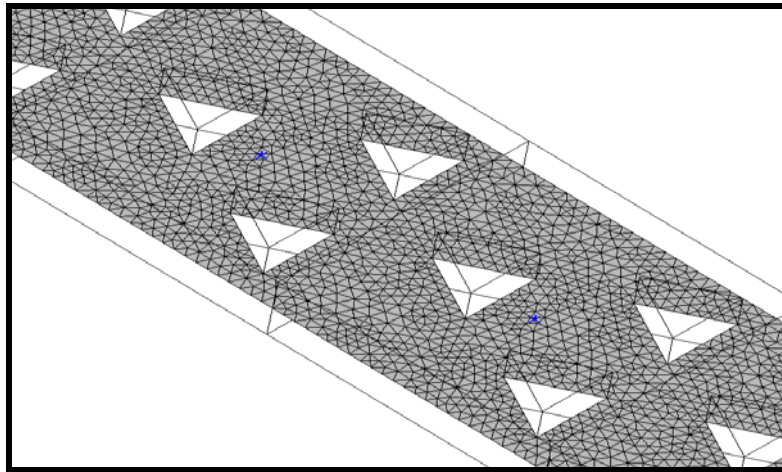
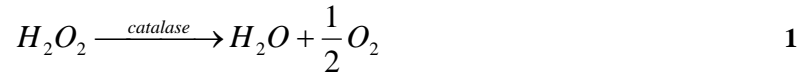


**Figure 2. Computational Grid Created to Model Original Physical Experimentation [3]**

Although the computational approach was validated using experimental data for the breakdown of urea into ammonia and carbon dioxide in the presence of urease, the equations used in the model are in no way limited to that specific enzyme/reaction combination.

The objective of the present study is to seek fundamental understanding of flow and chemical reaction behavior in a catalase bioreactor channel using CFD software. The reaction taking place involves hydrogen peroxide reacting with catalase to produce water and oxygen (dissolved). This is shown in Equation 1.



Recommendations are developed for design improvements due to this fundamental understanding. A series of six packing configurations that vary placement and number of triangular packing particles in a 500 $\mu$ m x 125 $\mu$ m x 10mm catalytically active microchannel are simulated and compared to the base case of an empty catalytically active microchannel. The surface area and dimensions of each individual packing element are held constant. Resulting flow fields are analyzed based on their ability to redistribute fluid and increase conversion by the end of the 10mm length. Consideration is given to pressure drop, residence time, and shear stress produced.

## Background

The physical bioreactor, on the order of hundreds of micrometers in size, is typically fabricated from a plastic material. Silicon wafers used by the microelectronics industry dominate as the fabrication material for these microreactors. However, the less expensive yet equally strong plastic material polydimethylsiloxane (PDMS) has been successfully used as well. For both

materials, the incorporation of enzyme may be accomplished in a number of ways. Newer, more efficient techniques of enzyme immobilization in microreactors were recently developed.

The experimental data that served as the basis for validating the use of the CFD numerical model were produced by two physical bioreactors, which were fabricated from silicon and PDMS with the enzyme urease entrapped in the walls. The fabrication and enzyme incorporation techniques involved in the experimentation are described in the following sections.

### **Microreactor Fabrication**

The microreactors referenced in this paper were fabricated using molds made by photolithographic techniques. Specialized design software called L-Edit allows the channels to be sketched as a “mask pattern” and then printed onto a transparency. The mask is drawn and printed to scale with an internal unit equivalent of 1 $\mu$ m. The mask is then placed on top of a SU-8 photoresist spun-coated silicon wafer and exposed to ultraviolet light, transferring the mask pattern. Chemically etching the exposed SU-8 produces a negative pattern of the microchannels with the precise geometry and dimensions of the mask pattern. This serves as a mold. Onto this, the material intended to form the reactor is poured and allowed to cure. The reactor is then peeled off the mold and put into use. Figure 3 summarizes these steps for microreactor fabrication. [2]

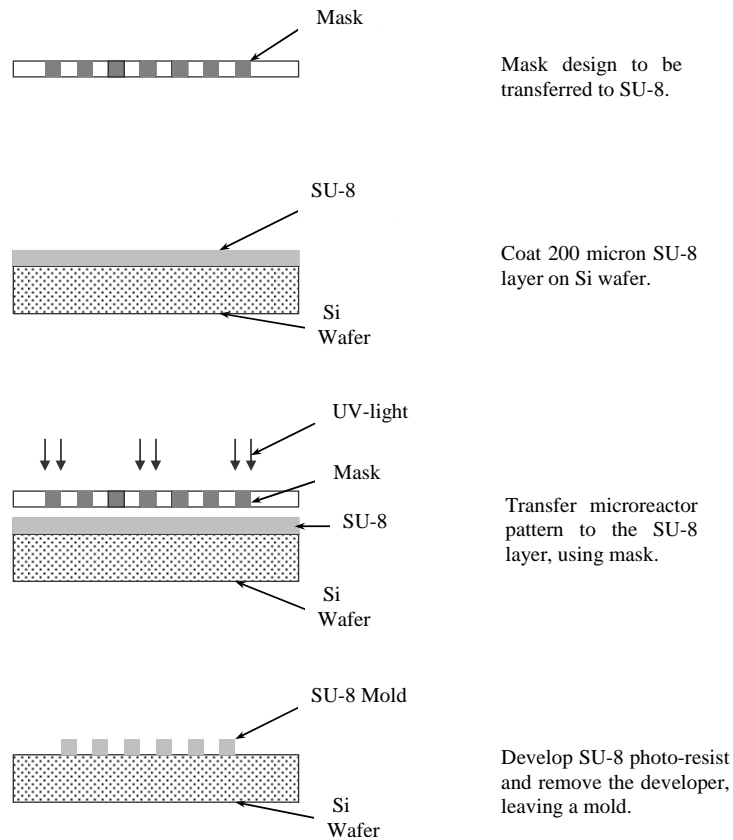


**Figure 3. Procedure for Microreactor Mold Fabrication (2)**

### PDMS-E Bioplastic Reactor

One way of fabricating a biomicroreactor is to make the material used to form the reactor catalytically active. In this case, a reactor material like PDMS is impregnated throughout with enzymes. This PDMS + enzyme mixture is then poured onto the mold in a layer about 5-8mm thick and allowed to cure for 3-5 days. In this way, enzymes are immobilized in the plastic and on the surfaces of the channel. Then the PDMS-E reactor is removed, sealed between two glass plates, and plumbed for use.

## Experimental Results from Supporting Literature

The experimentation on which the numerical simulation validation is based shows that under continuous-flow conditions, the PDMS-E biomicroreactors demonstrate increased conversions of urea with increases in residence time (time fluid spends in the reactive channel) and increases in enzyme loading (amount of enzyme incorporated into reactor). Also, in a 30 hour period of continuous operation, conversions are observed to decrease by about half and level off. [1]

A later study demonstrates that computational models can predict the associated conversions based on the increases in residence times and enzyme loadings [3]. Computational models of 0.01, 0.02, and 0.03 g of urease / g PDMS microreactors consisted of unstructured grids containing approximately 171,000 computational cells each [3]. Surface enzyme concentrations were calculated from the weight percent of enzyme and assumed uniform distribution of enzyme. Defining nine validation cases, three flow rates per microreactor, this study found that the simulation data represents reasonable upper and lower bounds for the experimental data when 10% and 100% enzyme activity are considered. Also, the overall trends exhibited by the experimental data are present in the computational findings [3]. Having confirmed the ability of the computational model to predict trends in experimental data, the enzyme and reacting fluid parameters were changed to those of catalase and  $\text{H}_2\text{O}_2$  respectively. The microchannel model for the reaction of  $\text{H}_2\text{O}_2$  with catalase to produce  $\text{H}_2\text{O}$  and  $\text{O}_2$  was then enhanced by the addition of internal features to demonstrate the use of the software as a design tool. Finding that the

presence of internal features within the reactor channels enhances the level of conversion reached at the outlet of the reactor more than could be attributed to the simple increase in enzyme active surface area, further study of micromixing was suggested [3].

A subsequent study, currently in submission [5], reports that this catalase bioreactor was successfully simulated over a broad range of flow rates. Using a repeating pattern of three triangular packing features, the study found that redistribution of the model's characteristically laminar (streamline and layered) flows significantly increases conversion over the entire range of flow rates ( $0.25 < Re < 62.5$ ) when compared with the conversions attained by empty channels. A peak improvement in conversion is found to occur at a Reynolds number near 20. Changing the mixing patterns significantly by reversing the flow into the bases of the triangles does not improve conversions, but the continued study of the effects of various flow obstruction configurations was suggested. This suggestion led to the present study.

## **Supporting Theory**

The simulation technique used to model microreactor behavior in the present study is characterized by governing equations that are differential in nature. The computational solver software, CFD-ACE+, finds solutions to these equations for each computational grid volume (computational cell) in the model. Boundary conditions are imposed on the microreactor surfaces, inlets, and outlets to model

enzyme coverage of internal surfaces and flow rates. The various inlet flow rates simulated are compared using the dimensionless parameter Reynolds number, since flow conditions and micromixing are studied. The following describes these in detail.

## **Governing Equations**

The flow, mixing, and heterogeneous liquid-solid reaction in the catalytically active microchannels are described by a complex set of coupled nonlinear partial differential equations. For this study, several assumptions are introduced that significantly simplify these equations:

- The density and viscosity of the reacting fluid are determined by its primary constituent, water. The very small concentration of the substrate (hydrogen peroxide) has no appreciable effect on these parameters. This small substrate concentration also negates the minimal amounts of heat produced in the reaction, so the system is considered to be isothermal.
- The fluid flow is steady state, incompressible, and characteristically laminar due to low fluid velocity and small dimensions of the channel.
- Chemical reactions are heterogeneous, taking place only at solid-liquid interfaces where enzyme is present.

With these assumptions the flow field (velocity and pressure gradients) within a reactor microchannel is determined by solving the following forms of the conservation of mass (continuity) and Navier-Stokes (momentum) equations:

$$\nabla \cdot \mathbf{V} = 0 \quad 2$$

$$\rho \mathbf{V} \cdot \nabla \mathbf{V} = -\nabla p + \mu(\nabla^2 \mathbf{V}) + \rho \mathbf{g} \quad 3$$

- where  $\mathbf{V}$  = Cartesian velocity vector (m/s)
- $\rho$  = bulk mixture density (kg/m<sup>3</sup>)
- $p$  = pressure (Pa)
- $\mu$  = bulk mixture absolute viscosity (N·s/m<sup>2</sup>)
- $\mathbf{g}$  = gravitational acceleration vector (m/s<sup>2</sup>)

The steady-state concentration field is described by

$$\mathbf{V} \cdot \nabla C_i - D_i \cdot \nabla^2 C_i = 0 \quad 4$$

- where  $i$  = species indicator (one equation for each species)
- $C_i$  = concentration of species  $i$  (M)
- $D_i$  = diffusivity of species  $i$  in solvent (m<sup>2</sup>/s)

The kinetics of the heterogeneous chemical reaction that takes place at the solid-liquid interfaces is described using the Michaelis-Menten model:

$$v = \frac{V_{\max} [S]}{k_m + [S]} \quad 5$$

- where  $v$  = reaction rate (mole/(s·m<sup>2</sup>))
- $[S]$  = substrate concentration at the solid surface (M)
- $V_{\max}$  = the maximum reaction rate (mole/(s·m<sup>2</sup>));  $V_{\max} = k_{cat} [E]$
- $k_m$  = Michaelis constant (concentration that gives  $v = V_{\max}/2$ ) (M)
- $k_{cat}$  = turnover number (s<sup>-1</sup>)
- $[E]$  = enzyme concentration at the solid surface (mole/m<sup>2</sup>)

## Boundary Conditions

The boundary conditions associated with flow and reaction in microchannels are as follows. At the channel inlet, a uniform velocity distribution and substrate concentration were specified, while at the channel exit, a fixed pressure boundary condition was assigned. A no-slip boundary condition ( $\mathbf{V} = 0$ ) was applied at all solid surfaces. If no enzyme is present on a solid surface, the concentration boundary condition is given by

$$D_s \frac{d[S]}{dn} = 0 \quad 6$$

where  $D_s$  = diffusivity of substrate in solvent ( $\text{m}^2/\text{s}$ )

$n$  = distance in direction normal to the solid surface (m)

If enzyme is present at the surface, the following boundary condition, which includes Michaelis-Menten kinetics, was applied to implement the steady, heterogeneous catalysis reaction:

$$-D_s \frac{d[S]}{dn} = \frac{V_{\max}[S]}{k_m + [S]} \quad 7$$

## Dimensionless Parameter

One dimensionless parameter is of particular interest in this study. This is the Reynolds number ( $Re$ ), given by

$$Re = \frac{\rho U d}{\mu} \quad 8$$

where  $U$  = velocity magnitude (m/s)

$d$  = smallest channel cross-dimension (m)

The Reynolds number represents the ratio of inertial forces to viscous forces within the moving fluid, and it is a determining factor in transition from laminar to turbulent flow. As already mentioned, all flows in this study are laminar.

## **Numerical Solutions Method**

The differential governing equations associated with momentum, mass, and chemical species conservation were solved numerically using the CFD-ACE+ computational package developed by ESI CFD Inc., located in Huntsville, Alabama [4]. CFD-ACE+ is a finite-volume-based code that employs a variation of the SIMPLEC (Semi-Implicit Method for Pressure-Linked Equations Consistent) algorithm [12]. As with all finite-volume methods, two major approximations are employed:

- The physical domain is broken down into a series of small control volumes (cells). The resultant collection of cells is referred to as the computational grid.
- The differential governing equations are replaced by a set of algebraic finite-difference equations that approximate the requirements of the differential equations in each cell.

In general, the velocity, pressure, and concentration fields are linked. The solution algorithm proceeds in two major steps. First, the velocities and pressures at the cell centers are calculated using an iterative pressure-correction approach (SIMPLEC). Once these flow field variables are determined, they are introduced into

the approximated species conservation equation, and the concentrations at the cell centers are calculated iteratively.

## **Design Simulation Details**

Data from physical testing of a catalase bioreactor that converts hydrogen peroxide to water and oxygen in the presence of the enzyme catalase was successfully modeled by CFD software in previous research [3]. The associated reaction is shown in Equation 1 in the Introduction section. The purpose of the present study is to begin optimization of a catalase bioreactor using computer simulation techniques. Optimization includes increasing the level of conversion reached at the exit of the reactor, finding the most efficient length of reactor needed, and finding the most efficient operating speed for the reactor. In the search for optimum operating conditions, a study of static micromixing (laminar fluid redistribution) and its effects on conversion within microreactor channels is the first step. Results of this type of study apply to other heterogeneous bioreactor systems and lend new fundamental information to the understanding of physical laws governing micromixing.

To study micromixing and its effects on conversion in microchannels, one microchannel design variation was chosen for experimentation. This design variation concerns the location and number of triangular packing particles added to the catalase bioreactor channels. A triangular shape was chosen for the packing because this shape divides flow and directs it towards enzyme active walls. Five packing

configurations, or patterns, were chosen with the expectation that they would contribute to a fundamental understanding of the nature of micromixing and aid in the optimization of microreactors. Figure 4 shows a top view of these patterns. When extruded into three dimensions, these  $500\mu\text{m} \times 500\mu\text{m} \times 125\mu\text{m}$  configurations form what are called unit cells. Each unit cell configuration is repeated 20 times to form the full 10mm length of its respective channel. The channels and their respective configurations are referred to as (1) Empty, (2) One Triangle, (3) Two Triangle Asymmetric, (4) Two Triangle Inline, and (5) Three Triangle.

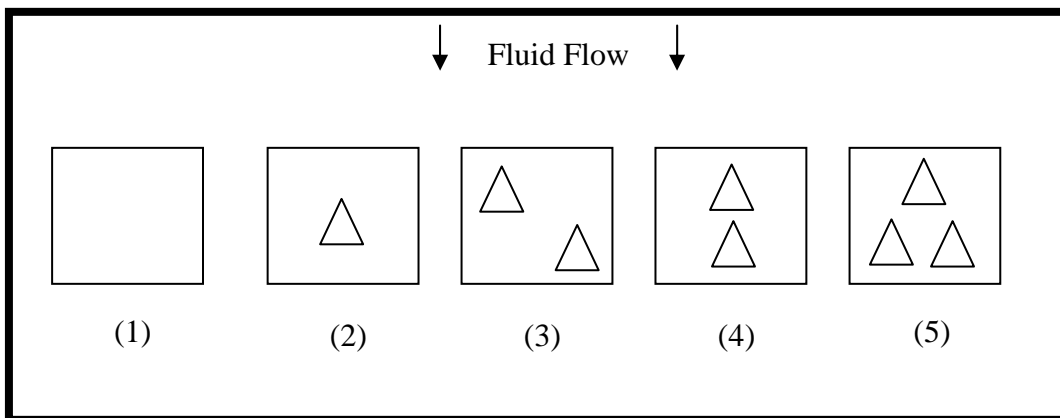


**Figure 4. Microchannel Obstruction Configurations**

An additional study was prompted by the results of this initial set of configurations. The additional study added two more configurations that each consisted of two triangles. This allowed for a comparison of the performance of four different two triangle configuration designs, shown in Figure 5.

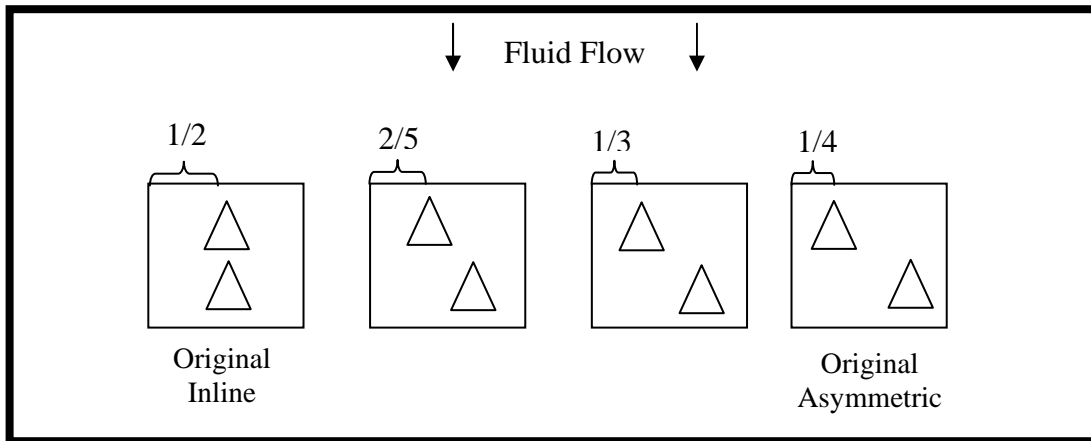


**Figure 5. Microchannel Configurations: Study Concerning Effect of Two Triangle Placement**

The Two Triangle Inline and Two Triangle Asymmetric configurations from Figure 4 are repeated in Figure 5 (for purposes of comparison) at the left and right ends of the diagram respectively. The measurements above the unit cells in Figure 5 show the placement of the front points of the triangles in each configuration with respect to the channel width. These unit cell configurations are referred to as Two Triangles Inline, Two Triangles 2/5, Two Triangles 1/3, and Two Triangles 1/4 according to the location of their packing.

Previous research modeled and compared the empty and three triangle configurations as  $500\mu\text{m} \times 125\mu\text{m} \times 50\text{ mm}$  biomicroreactors [3]. Limitations of the computing power available to run these simulations resulted in a fairly sparse grid. Thus the intricacies of flow development and chemical behavior occurring in the beginning of the channels were lost. Additionally, in some cases nearly complete conversion of the reacting fluid occurred long before the end of the 50mm channel.

The bioreactor channels modeled for the present study were shortened to 10mm in length so that a computational grid five times as dense as the previous research could be used. This allows for smaller computational grid volumes lending more accuracy to the numerical solutions of the governing equations. Approximately one million computational cells were used in each microchannel grid. This number of computational cells approaches the maximum computing power available. Each computational cell is solved multiple times (iterated) until a stable solution is reached. A Dell Precision 670 server with an Intel Xenon 3.6GHz processor and 3GB Ram is used as the computing machine. A summary of the number of computational cells, iterations, and computing times is shown in Table 1.

**Table 1. Microchannel Grid Parameters**

Channel Type	Re	Number of Computational Cells	Total Iterations	CPU Time (hr)
<b>Empty</b>	0.1	944,370	40000	244.4
	1	944,370	4500	48.9
	10	944,370	3000	32.6
	100	944,370	6000	65.2
<b>1 Triangle</b>	0.1	968,940	7000	76.1
	1	1,107,840	12000	130.4
	10	1,107,840	5800	63.0
	100	1,107,840	2000	21.7
<b>2 Triangle Inline</b>	0.1	1,109,218	3000	32.6
	1	1,068,914	9033	98.1
	10	1,068,914	3022	32.8
	100	1,068,914	2500	27.2
<b>2 Triangle Asymmetric 1/4</b>	0.1	1,107,840	2250	24.4
	1	1,092,916	9000	97.8
	10	1,092,916	3000	32.6
	100	1,092,916	1985	21.6
<b>2 Triangle Asymmetric 1/3</b>	0.1	1,092,916	3848	41.8
	1	1,111,264	6300	68.4
	10	1,111,264	5000	54.3
	100	1,111,264	1050	11.4
<b>2 Triangle Asymmetric 2/5</b>	0.1	1,111,264	1500	16.3
	1	1,109,218	6632	72.1
	10	1,109,218	3500	38.0
	100	1,109,218	3500	38.0
<b>3 Triangle</b>	0.1	1,041,140	7500	81.5
	1	1,041,140	3000	32.6
	10	1,041,140	2000	21.7
	100	1,041,140	2000	21.7

A total of 56 computer simulations were performed with the unit cell designs shown in Figure 4 and Figure 5. This number does not include other simulations used in a grid study to optimize computational cell placement. In the study presented, each channel configuration is simulated for flow and chemistry solutions sequentially (due to the constraints of the computing power available). The inlet concentration of H<sub>2</sub>O<sub>2</sub> is held constant at 0.0147M H<sub>2</sub>O<sub>2</sub> in water. Additionally, each configuration is

simulated at four Reynolds numbers, 0.1, 1, 10, and 100, which correspond to fluid inlet velocities of 0.001048, 0.01048, 0.1048 & 1.048 m/s. Table 2 gives the parameters used in the CFD model.

**Table 2. Flow, Mass Transfer, and Kinetic Parameters**

Property	Symbol	Value
Bulk mixture density [14]	$\rho$	998 kg/m <sup>3</sup>
Bulk mixture kinematic viscosity [14]	$\nu$	1.31x10 <sup>-6</sup> m <sup>2</sup> /s
Diffusivity of H2O2 in water	$D_i$	1.0x10 <sup>-9</sup> m <sup>2</sup> /s
Michaelis constant for breakdown of H2O2 catalyzed by catalase [15]	$k_m$	0.025 M
Turnover number for breakdown of H2O2 catalyzed by catalase [15]	$k_{cat}$	1.0x10 <sup>7</sup> s <sup>-1</sup>

These simulations produced flow velocity fields and conversion information that are presented and discussed in the following section.

## Results and Discussion

The reaction environment of the simulated microchannels is characterized by heterogeneous catalysis of the flowing fluid. The conversion of the fluid from H<sub>2</sub>O<sub>2</sub> to H<sub>2</sub>O and O<sub>2</sub> depends on its contact with the enzyme-active walls as well as residence time and the reaction rate of the enzyme catalase. Improving this heterogeneous reaction environment requires fluid redistribution to the walls. The performance of the various packing configurations shown in Figure 4 and Figure 5 is

investigated for mixing, reaction conversion, pressure drop, and shear stress at the walls.

## Effect of Design on Fluid Redistribution

### *Empty Channel*

The simulation of an empty channel biomicroreactor with no packing serves as a basis for comparison of the various design configurations tested and reported in this study. The flow pattern produced at the inlet of the empty channel at various Reynolds numbers is shown in Figure 6 with shaded velocity fields.

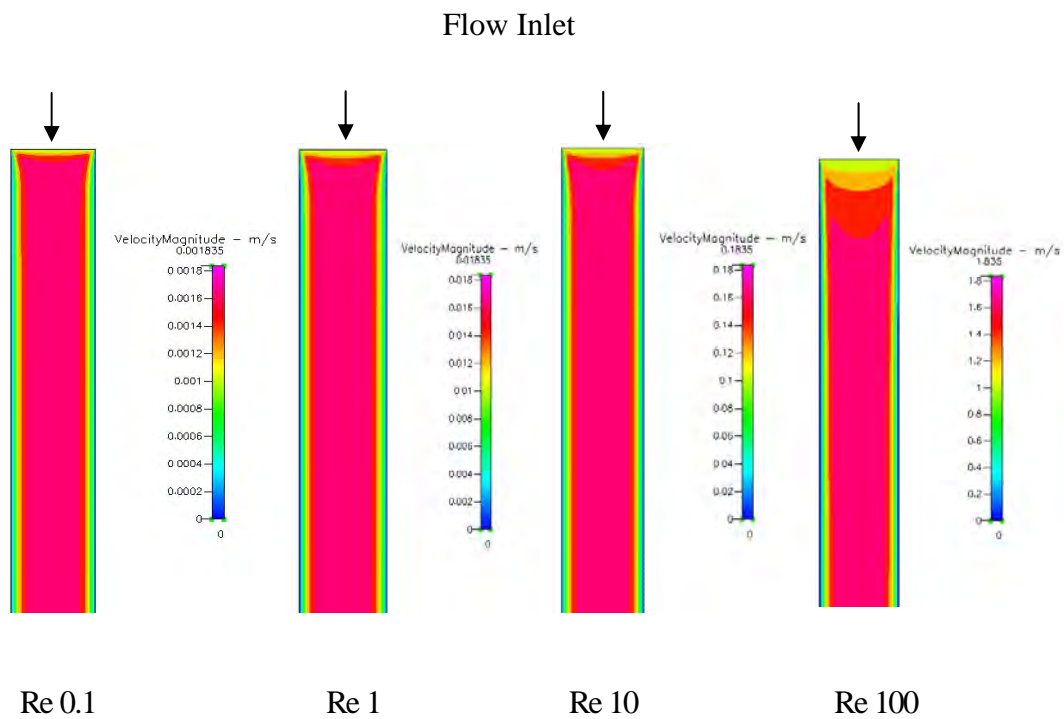


**Figure 6. Inlet Flow Field of Empty Microchannel at Various Reynolds Numbers**

These flow fields represent a top view of a horizontal slice through the channel's midline. Here, the highest fluid velocity (red) flows down the center of the channel while the boundary layer produced by the surface drag of the walls (blue) slows the fluid significantly on either side. This flow pattern is characteristic of a laminar flow regime. The velocity fields develop quickly due to the slowness of the flows. Empty channel simulations produce levels of conversion that decrease as Reynolds number increases. Figure 7 shows a cross-sectional view of the H<sub>2</sub>O<sub>2</sub> concentration gradients at the exit of the empty channel for the four Reynolds numbers simulated.

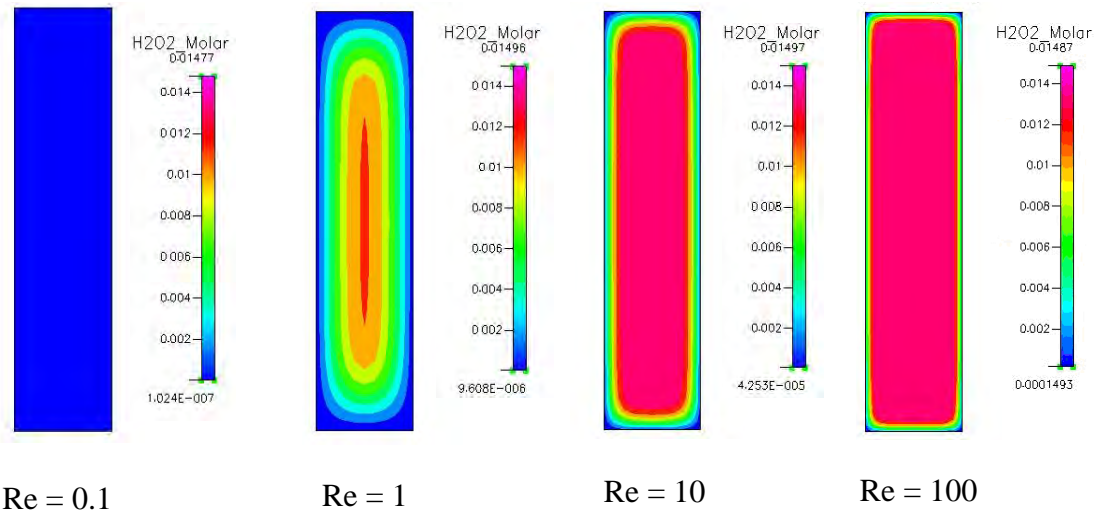


**Figure 7. Outlet Conversion Fields of the Empty Channel at Various Reynolds Numbers**

The blue regions shown in this figure represent fully reacted fluid. For the slowest flow (Re = 0.1), there is complete conversion. As Re is increased, the central unreacted regime grows outward. These patterns are a result of the only micromixing mechanism present, diffusion. Since diffusion is time dependent, increases in fluid

velocities result in decreases in residence time and effective diffusion. For increasing Reynolds numbers, the levels of conversion of  $\text{H}_2\text{O}_2$  to  $\text{H}_2\text{O}$  reached by the exit of the channels are 98.7%, 43.0%, 9.84%, and 1.97% respectively. Figure 8 gives a graphical representation of this effect.

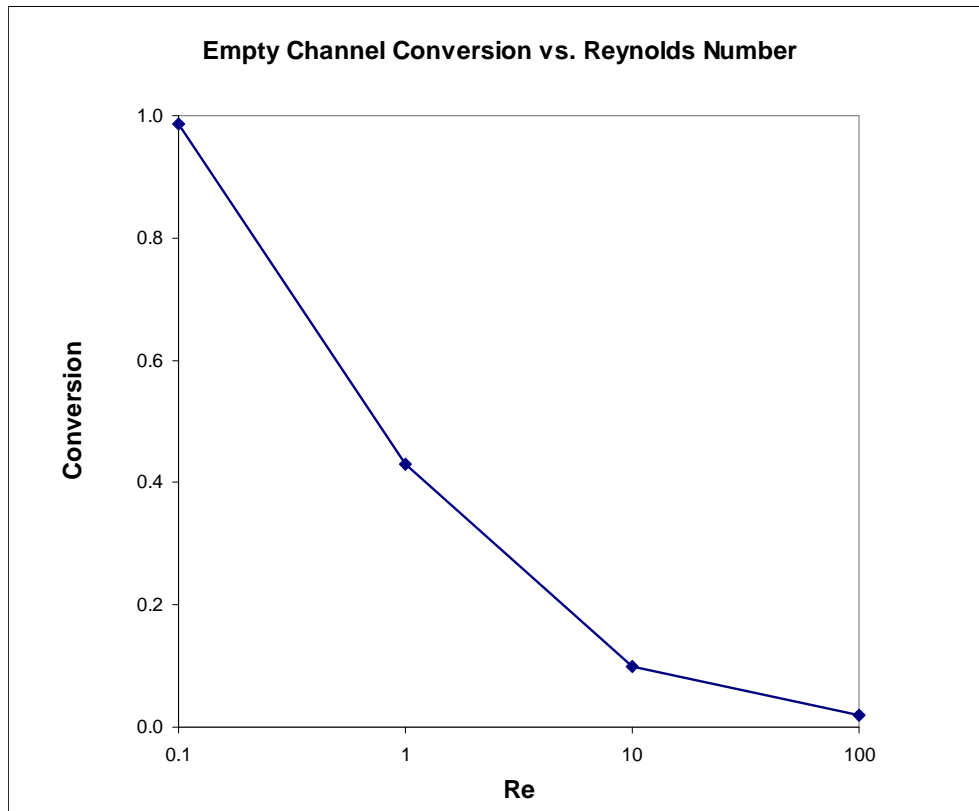


**Figure 8. Effect of Fluid Velocity on Conversion in Empty Channel**

At a Re of 0.1, high conversion is expected since this corresponds to a fluid inlet velocity of 0.001048 m/s. Under such conditions, a high residence time of 9.54 seconds allows diffusion of reactants to the walls for catalysis by enzymes. An order of magnitude increase to a Re of 1 produced less than half the conversion attained in

creeping flow conditions due to the reduction in residence time and therefore reduction in the effectiveness of diffusion.

Complete conversion could have been reached for each Reynolds number by lengthening the channels thereby increasing residence time and diffusion. However, in this study flow obstructions are added to aid in the redistribution of the reacting fluid to the enzyme-active walls. This is intended to increase conversion while keeping reactors small. Smaller reactors that can accomplish the same level of conversion are cheaper to fabricate and therefore preferable.

### *One Triangle Configuration*

In the case of configuration 2, a single triangular packing particle is added per unit cell to cause some fluid redistribution and to add reactive surface area. Inlet region velocity fields for this design are shown in Figure 9.

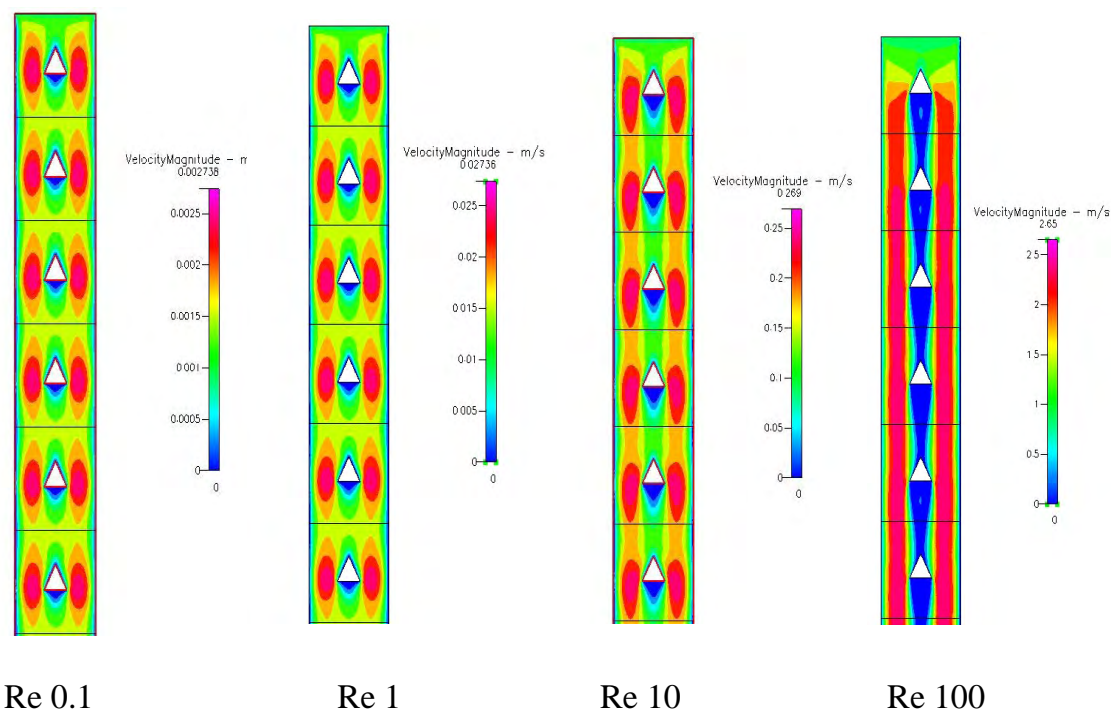


**Figure 9. Inlet Flow Fields of Microchannel with One Triangle per Unit Cell**

The advantage of this configuration over the empty channel is visible in Figure 9.

Fluid is directed to the reactive outside walls carrying reactants that might not otherwise have diffused there. The reduction in flow cross-sectional area due to each triangle causes an increase in velocity within the channel and likewise a higher Reynolds number in certain regions. Also, the surfaces of the triangles are enzyme active, presenting more reactive surface area to the flow. Although each triangle covers some surface area of the channel's enzyme-active top and bottom planes, each adds 5.6% active surface area to each unit cell.

Table 3 summarizes the channel metrics, such as volume and reactive surface area, for each packing configuration.

**Table 3. Channel Metrics**

Channel Type	# triangles	Reactive Flow Volume (mm <sup>3</sup> )	Enzyme-Active Surface Area (mm <sup>2</sup> )	% Extra Enzyme Area	Reynolds number	Residence Time (sec)	Shear Stress (N/m <sup>2</sup> )
empty	0	0.625	12.5	0	0.1	9.54	0.09
					1	0.95	0.90
					10	0.10	9.11
					100	0.01	97.88
1 triangle	1	0.603	13.2	5.6	0.1	9.21	0.11
					1	0.92	1.08
					10	0.09	11.29
					100	0.01	141.53
2 triangle inline	2	0.581	13.9	11.2	0.1	8.88	0.13
					1	0.89	1.28
					10	0.09	13.15
					100	0.01	152.67
2 triangle asymmetric 1/4	2	0.581	13.9	11.2	0.1	8.88	0.15
					1	0.89	1.47
					10	0.09	16.41
					100	0.01	318.21
3 triangle	3	0.559	14.6	16.8	0.1	8.54	0.21
					1	0.85	2.11
					10	0.09	24.63
					100	0.01	606.36

For the One Triangle case, a 3.5% reduction in the volume of the channel due to the addition of the obstructions causes some disadvantages. For one, a decrease in flow area will increase velocity and hence shear stress. Also, as seen in Figure 9, increasing the Reynolds number results in larger wake regions (blue). Packing causes significant increases in pressure drop as well. This is presented in a later section.

The wake and flow patterns produced by the One Triangle configuration at Re 100 are distinctly different from those at the lower Re of 0.1, 1, and 10, which are very similar to each other. The high velocity regions seen in the flow fields of the lower Reynolds number simulations merge at Re 100 to form two high velocity streams on the left and right sides of the channel. The straightness of these two

streams and the merging of the blue wake regions indicate that little cross-channel redistribution is occurring. Figure 10 shows an enlarged view of the resulting velocity vectors in the One Triangle unit cell at Re 10 and 100.

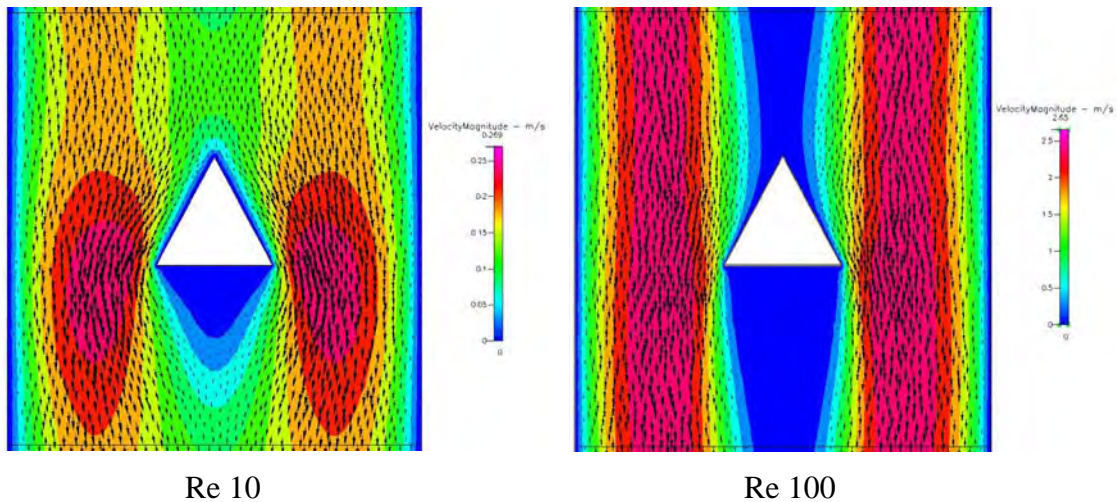


**Figure 10. Velocity Vectors in One Triangle Unit Cell at Re 10 and 100**

Somewhere between Re 10 and Re 100, the fluid flow in the channel breaks into a new regime. This new regime has various consequences for conversion, pressure drop, and shear stress inside the channel, which deviate from the patterns established by the lower Reynolds number cases. These phenomena are discussed in depth in later sections.

### *Two Triangle Inline Configuration*

A second obstruction was added to each unit cell. This configuration consists of two triangles inline in the center of each unit cell. This arrangement and the resulting flow fields are shown in Figure 11.

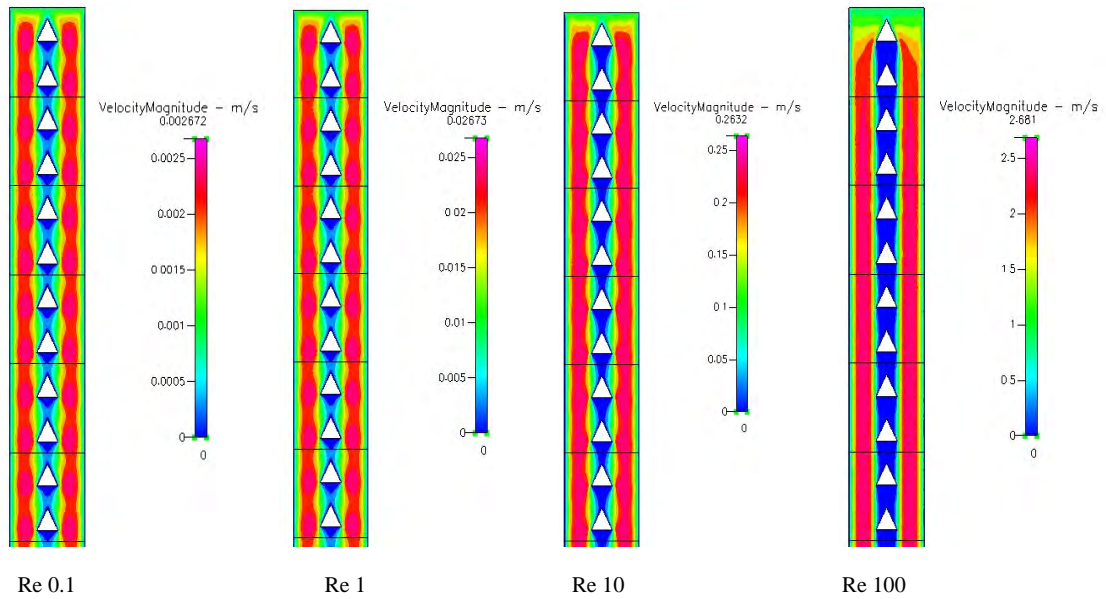


**Figure 11. Inlet Flow Field of Two Triangle Inline Microchannel at Various Reynolds Numbers**

The flow patterns at the lower three Re display high velocity streams on either side of the obstacles. This pattern lacks desirable cross-channel redistribution in that the large wake regions prevent fluid from crossing the mid-plane of the channel. A comparison of these flow fields to those with a single triangle are shown in Figure 12.

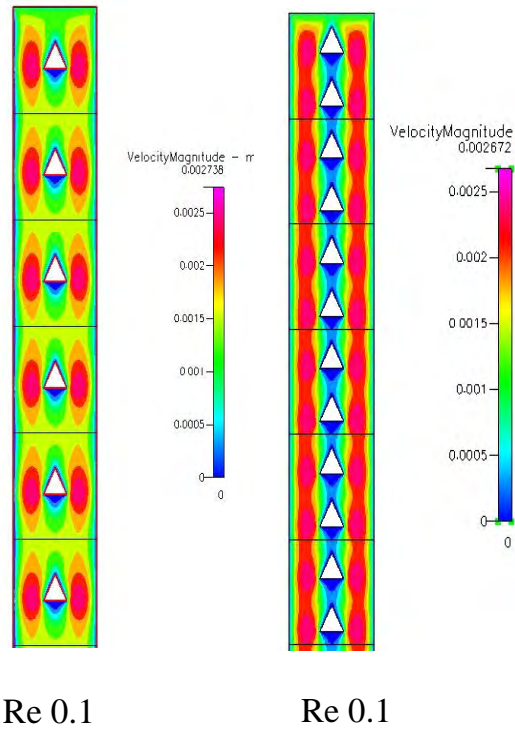


**Figure 12. Comparison of Flow Fields of Configurations 2 & 3**

In the Two Triangle Inline case, the obstacles and their wakes merge together even at the lowest Re, reducing the flow between the triangles and increasing the amount of fluid forced to the walls. The larger surface presented by the walls make this desirable in the case of heterogeneous catalysis. Nonetheless, increased resistance to flow results from the added objects, and pressure drop and shear increase accordingly.

### *Two Triangle Asymmetric Configuration*

Another two triangle unit cell configuration was studied with the intention of improving channel mixing by inducing cross flow. The original Two Triangle Asymmetric channel (configuration 4) is shown in Figure 13. Here, the two triangles

are placed in an asymmetric arrangement with each triangle centered in opposite quadrants of each unit cell (1/4 of the width of the channel from the walls). This arrangement places the upstream point of each triangle mid-way from the side wall to the channel centers.

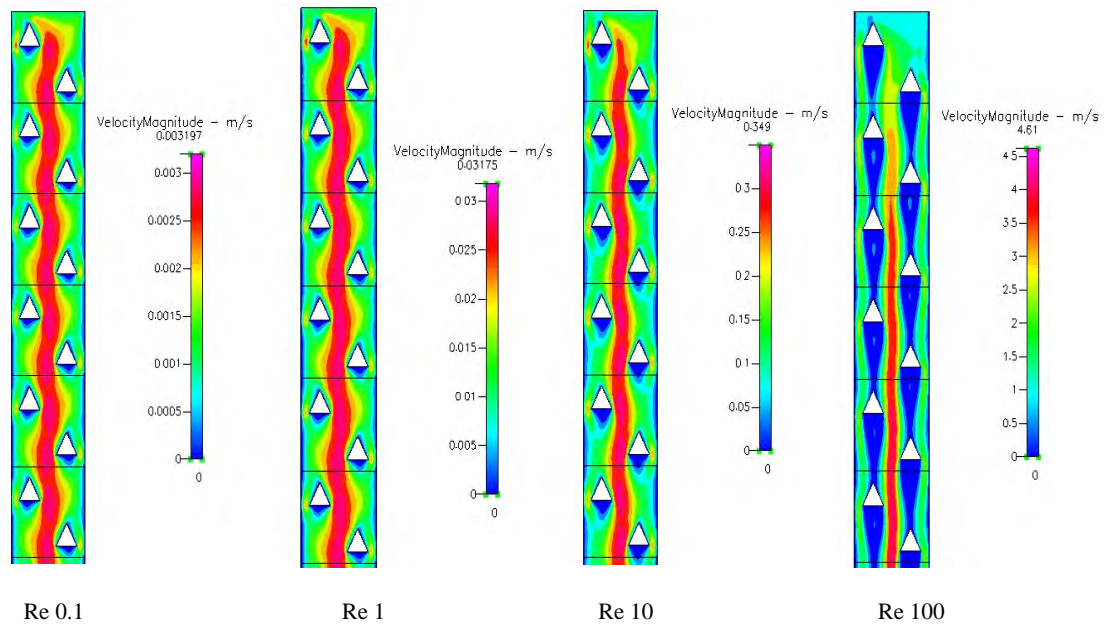


**Figure 13. Inlet Flow Fields of Two Triangle Asymmetric Microchannel at Various Reynolds Numbers**

Some channeling down the center of these microchannels is displayed and becomes increasingly more pronounced with increases in  $Re$ . The serpentine shape of the highest velocity fluid at  $Re$  0.1 indicates some fluid flows in the cross-channel direction, while most of it is channeled down the center. At  $Re$  100, the central channel of fast flow becomes straighter, and the wake regions grow. In this flow regime there is poor cross-channel fluid redistribution. However, there is a buildup of medium flow (green) along the side walls.

### Three Triangle Configuration

A third triangle is added to each unit cell to increase mixing and to present more surface area to the process fluid. The resulting flow fields are shown in Figure 14.

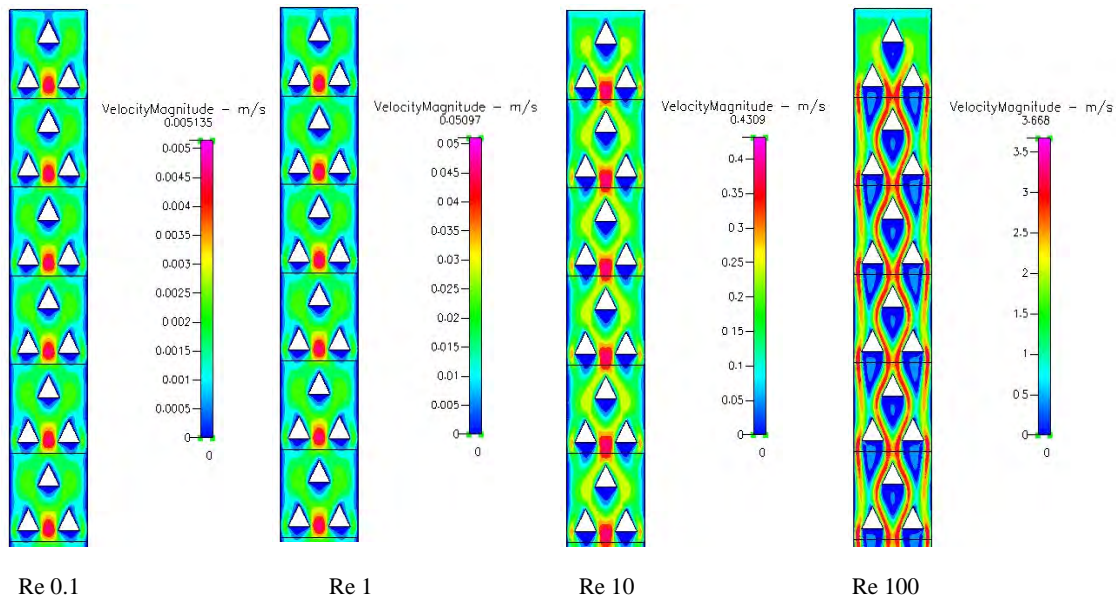


**Figure 14. Inlet Flow Field of Three Triangle Microchannel at Various Reynolds Numbers**

At the three lower Reynolds numbers, the fastest flows (red) occur in the open center of the channel between triangles. These flows are split by the centered triangle of the next unit cell and directed along its sloped sides, at which point cross-channel mixing occurs at a reduced medium speed (green and yellow). The slow flows along the side walls (blue) are interrupted by the medium velocity flows because the last two triangles in each unit cell force flow closer to the walls. A superior flow pattern arises at Re 100 with significant flow both around the center triangles and along the side walls. Also, the wake regions associated with drag on the triangles grow

dramatically, but do not intersect. These flow patterns are promising for heterogeneous catalysis since they direct fluid to all reactive surfaces.

### Effect of Design on Conversion

Variations in packing configurations are found to significantly affect conversion. For each case where fluid is redistributed in a cross-channel direction toward catalytically active side walls, higher percentages of  $H_2O_2$  are converted compared to the empty channel case. Figure 15 is a log-log plot of the percent conversion of  $H_2O_2$  versus Reynolds number for each of the configurations.

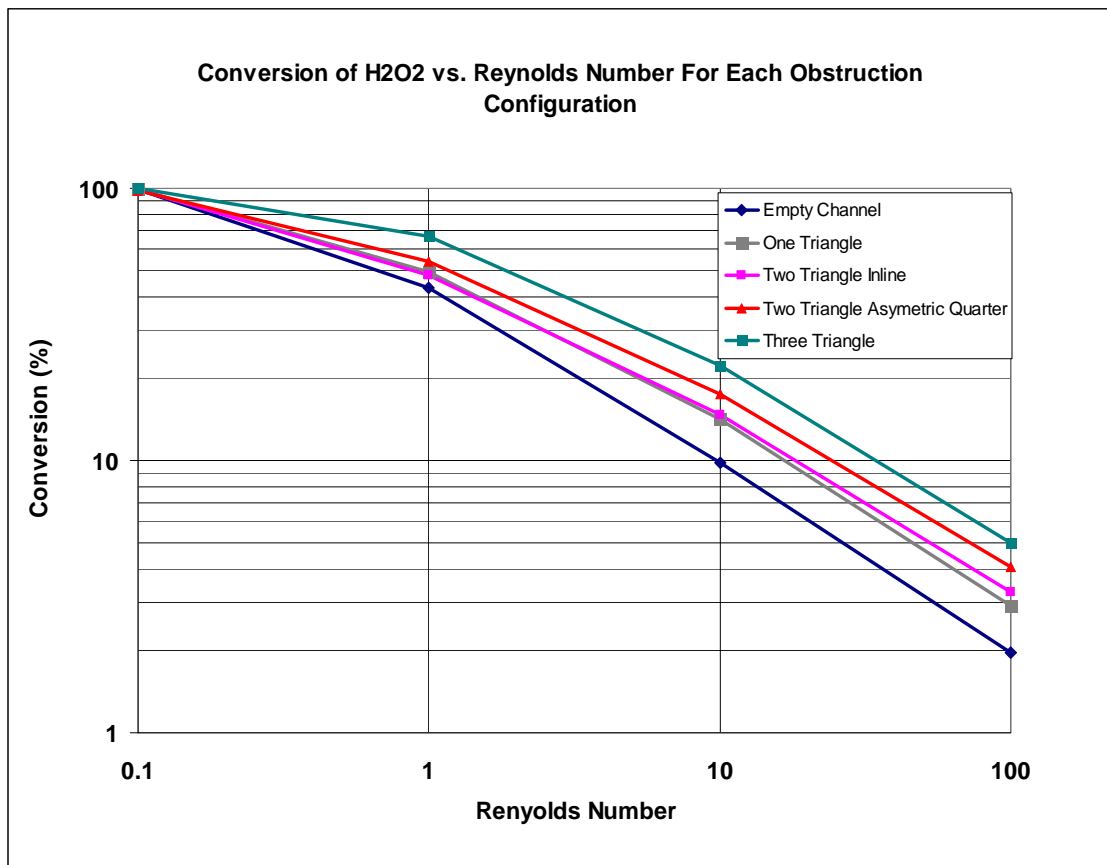
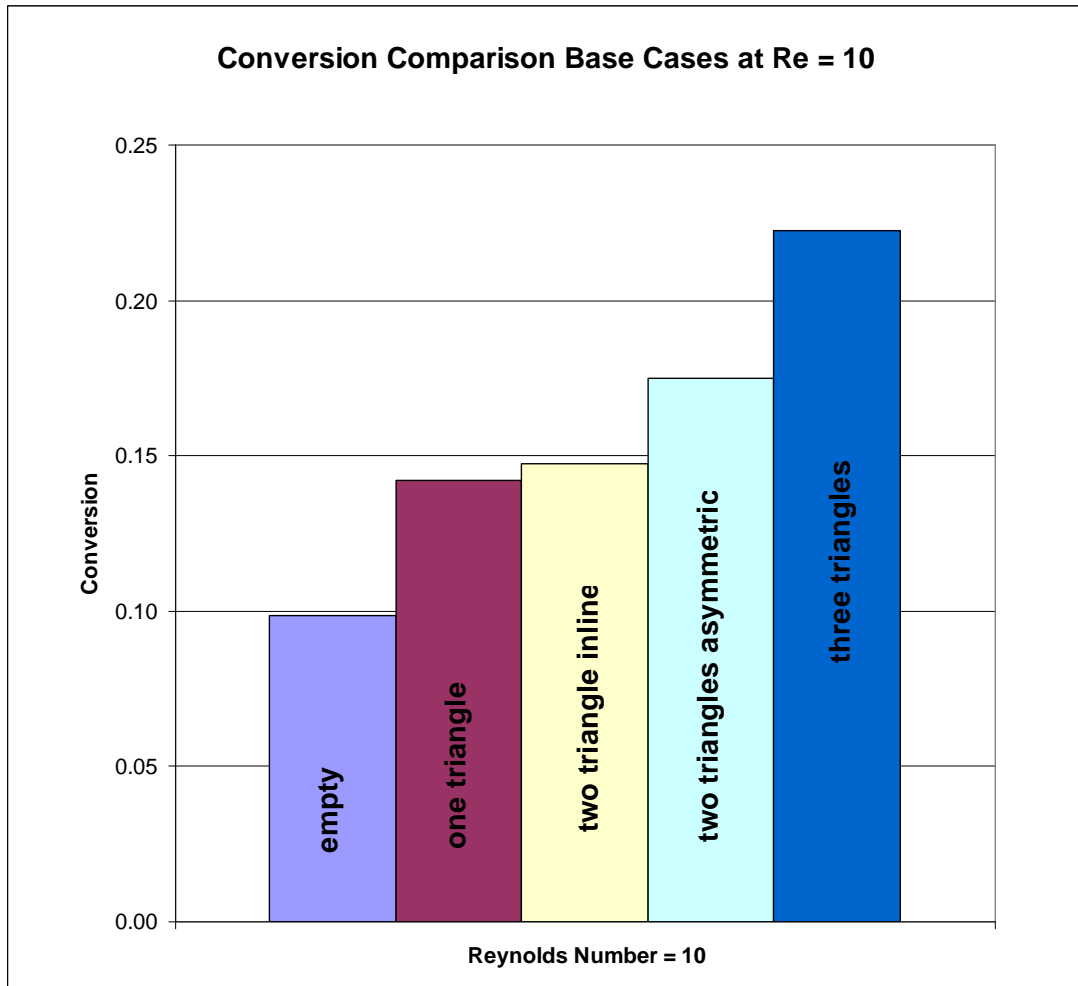


Figure 15. Effect of Flow Rate on Conversion for Various Packing Configurations

At a Reynolds number of 0.1, all of the configurations performed equally well due to creeping flow and long residence times. Slow flows give enough diffusion time for all reactants to reach reactive surfaces before exiting the channels. In some of these cases, complete conversion may have been reached before the end of the channel. A bar graph showing conversion levels is given in the Appendix (Figure A1).

In all cases, when a packing element is added there is a significant increase in conversion beyond the 5.6% additional surface area. For example, at  $Re = 10$  the channel configurations perform as shown in Figure 16.



**Figure 16. Comparison of the Effect of Packing Configuration on Conversion at Re=10**

At this Reynolds number, the effect of diffusion on conversion is minimal, but increased fluid redistribution is achieved by the addition of packing. An increase in conversion as high as 150% may be achieved by the addition of packing. From Figure 16, the addition of one triangle gives a 44% increase in conversion over the empty channel. From Table 3, this configuration corresponds to a 5.6% increase in enzyme-active surface area, clearly indicating that the benefit of much higher conversion outweighs the cost of extra enzyme.

The addition of two triangles to the base case produces increases of 49% or 78% conversion depending on the placement of the triangles. The lower of these conversions results from the flow field produced by the inline arrangement (Figure 11), where nearly straight channeling along either side of the packing and connected wake regions allow no cross-channel fluid redistribution. The higher number results from a flow field that is more effective at cross-channel redistribution, but still channels most of the fluid down the center (Figure 13). These two triangle configurations correspond to an 11.2% increase in enzyme-active surface area, which indicates a high benefit to cost ratio.

The addition of three triangles to the base case, which corresponds to a 16.8% increase in enzyme-active surface area, gives a 125% increase in conversion (Figure 16). This is the most beneficial arrangement of triangles for the reaction environment simulated. The resulting flow field shows great fluid redistribution and high velocity flows near the channel walls.

A bar graph for  $Re = 1$  is given in the Appendix (Figure A2). At  $Re = 1$ , the empty channel produces 43% conversion of  $H_2O_2$ . This is 43% of the conversion that was achieved at  $Re = 0.1$  showing that at this flow rate diffusion is still significant. Also, the increases due to packing are more modest (14% for one triangle, 12% and 26% for two triangles, and 56% for three triangles) than at  $Re = 10$  since mixing at such a slow flow rate is less significant. At  $Re = 1$ , the one triangle configuration produced increases in conversion compared to the empty channel of only 14%. The two triangle inline and the two triangle asymmetric configurations produced increases

in conversion of 12% and 26% respectively, and the three triangle configuration produced an increase of 54%. Although slight differences in volume and amount of enzyme are present for these cases (Table 3), the differences in conversion effectiveness result from the same criteria of effective flow fields as discussed for  $Re = 10$ . As stated previously, each configuration's flow field regime remains rather similar for  $Re = 0.1, 1, \text{ and } 10$ .

For the highest  $Re$  of 100, low levels of conversion were typical of all the configurations due to very small residence times of about 0.01 seconds (Appendix, Figure A3). Very little diffusion time is allowed at this fluid velocity, so the fluid redistribution accomplished by packing is the main factor effecting conversion. Although all the conversions were relatively small, the one triangle configuration produced an increase in conversion of 48% compared to the empty channel. Again, this configuration corresponds to an increase in enzyme-active surface area of 5.6%, meaning that the addition of the single packing particle to each unit cell is extremely effective. The flow field (Figure 9) for  $Re 100$  shows that the wake regions of the packing particles merge, forcing all fluid to either side of the channel. This in effect pushes more fluid to the outside walls for reaction. The two triangles inline configuration produced a 67% increase in conversion, while the two triangles asymmetric gave a 106% increase. The superiority of the two triangles inline configuration over the one triangle configuration at  $Re 100$  can be explained by the redistribution of more of the bulk flow to the outer walls. In comparing their flow fields (Figure 10 and Figure 11), the closer proximity of the two triangles inline

configuration created a wide, uniform wake region through the center, while the one triangle configuration allowed some of the bulk fluid flow to drift towards the middle of the channel and stagnate there. The dramatic difference between the effectiveness of both two triangle configurations can be solely attributed to their flow fields.

Figure 11 shows the inline arrangement at Re 100 with most of its flow space (near the walls on either side of the packing) occupied by high velocity. While this may seem beneficial, the flow field produced by the two triangle asymmetric configuration (Figure 13) shows medium velocity fluid (green) near the walls. Although some fluid at high velocity channels down the center, the slower fluid near the walls has more time to react and diffuse. Again, these two triangle configurations correspond to an 11.2% increase in enzyme-active surface area. Compared to the addition of one triangle to the base case (which gave an increase in conversion of 48%) adding another triangle in an asymmetric arrangement more than doubled the percent increase in conversion (giving 106% increase).

The Three Triangle configuration proved to be the most effective in terms of conversion. It produced a 154% increase in conversion compared to the base case empty channel, and had only a 16.8% increase in enzyme-active surface area (Table 3). Its flow field at Re = 100 shows high velocity flows near the walls and through the spaces of the packing. The associated wake regions do not merge, and are actually smaller than any of the other wake regions that do merge. This allows cross-channel redistribution to occur. Also, medium velocity fluid (green) fills the majority of the space allowing for more reaction and diffusion time.

The stark differences in the performance of the two cases that involved two triangles provoked a separate study of two triangle positioning within the channel. The results of this investigation are presented in the following sections.

### **Effect of Triangle Position on Fluid Redistribution**

#### *Two Triangle Asymmetric 2/5 Configuration*

The positions of two triangles (per unit cell) were logically varied to determine an optimal placement for chemical conversion. In the first variation, the triangles are shifted inward to  $2/5$  of the width of the channel. That is, the leftmost triangle point is  $2/5$  the width of the unit cell from the left wall and the rightmost triangle is  $2/5$  the width of the unit cell from the right wall. This arrangement and the resulting flow fields at various Reynolds numbers is shown in Figure 17.

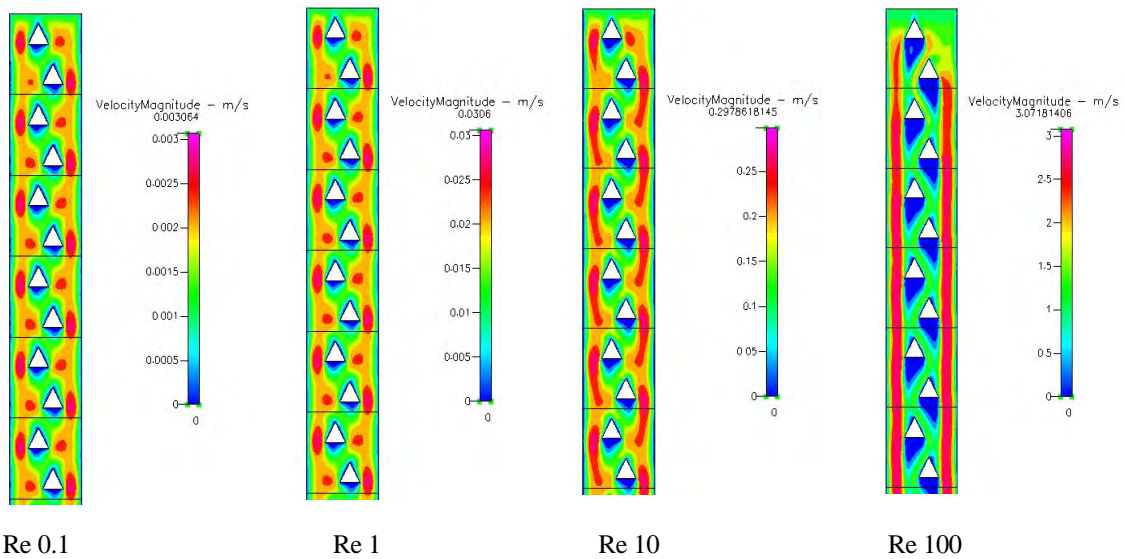


**Figure 17. Inlet Flow Fields for Two Triangles, 2/5 of Channel Width Away From Outside Walls**

The red fluid flows indicate the high velocities of fluid near the outside walls. The serpentine flow patterns produced on either side of the channel indicate improved cross-channel mixing compared to the original two triangles inline and two triangles asymmetric configurations. Most of the high velocity fluid remains on the outer sides of the triangles, however. Re 100 produces a flow regime with straight, solid fast flows along the walls.

### *Two Triangle Asymmetric 1/3 Configuration*

A second re-design of the two triangles asymmetric channel places the triangles' points 1/3 of the width of the unit cell from the left and right walls of the channel. In the resulting arrangement, the front-most points of the triangles divide the fluid flow into three equal regions. This can be seen in Figure 18 where the resulting flow fields are presented.

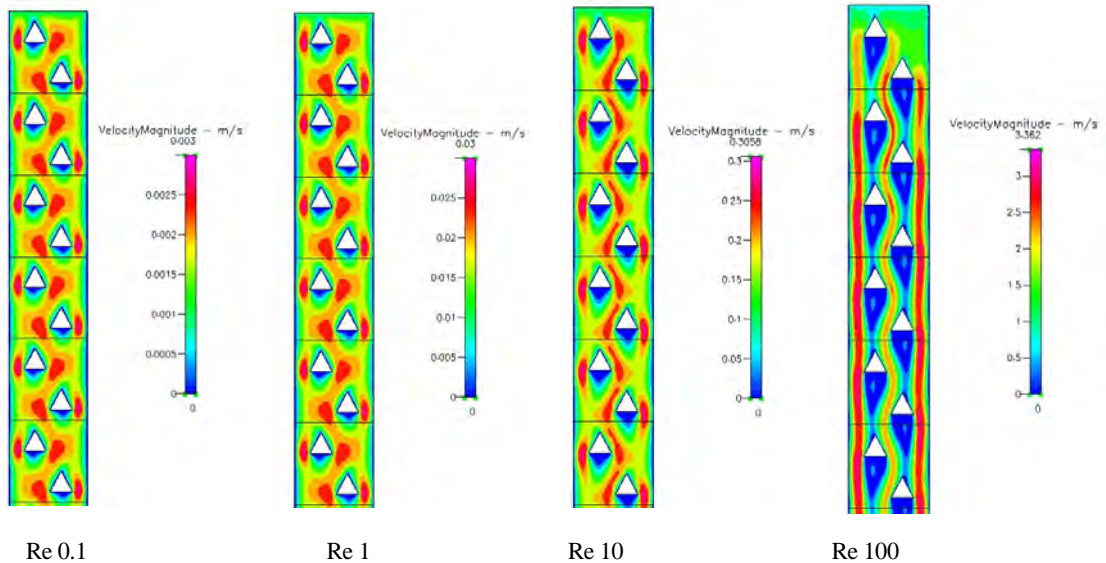


**Figure 18. Inlet Flow Fields for Two Triangles, 1/3 of Channel Width Away From Outside Walls**

The flow patterns for this configuration show the best patterns for fluid redistribution of any of the two triangle cases. High velocity flow (red regions) is directed to more surfaces and its serpentine paths are wider and farther reaching, producing greater cross-channel species redistribution. Even at Re 100, with its highly channeled flow regime, the main fluid streams are directed along all the major flow surfaces except the back walls of the packing.

A side-by-side comparison of the various two triangle configurations at Re = 0.1 (Figure 19) reveals the effect of obstacle placement on fluid redistribution more clearly.

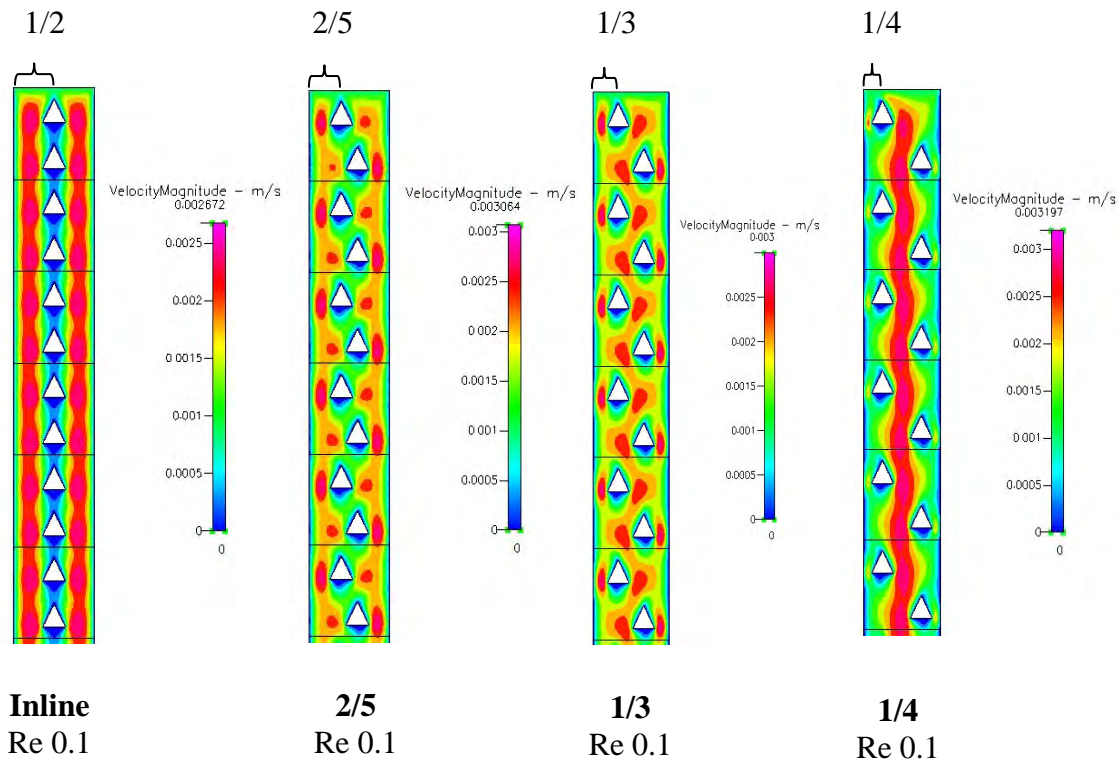


**Figure 19. Flow Field Comparison of Two Triangle Variations at Re = 0.1**

The inline and 1/4 configurations prove to be the extreme cases where fluid redistribution is minimal.

### **Effect of Triangle Position on Conversion**

Since each two triangle configuration contains the same number of obstacles and the same enzyme coverage, a direct comparison of the effect of triangle placement on conversion, pressure drop, and shear is possible. The conversion performance of each of the two triangle design configurations varied according to the degree of fluid redistribution. Figure 20 is a log-log plot of percent conversion of  $H_2O_2$  versus Reynolds number for each of the configurations.

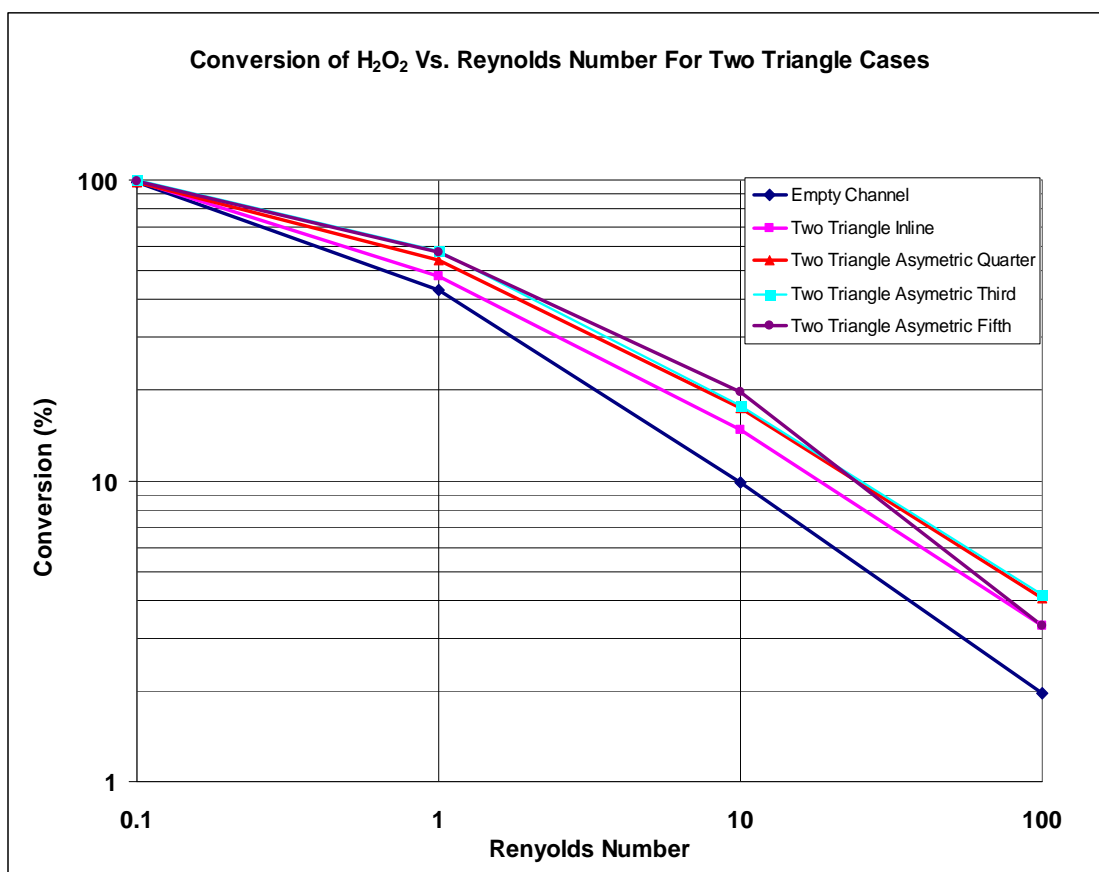


**Figure 20. Comparison of the Effect of Two Triangle Obstruction Configurations on Conversion**

At  $Re = 0.1$ , each configuration reached complete conversion by the end of the channel. A bar graph comparing conversion levels at this  $Re$  is shown in the Appendix (Figure A4). At higher  $Re$ , significant differences in conversion levels occur. Still more interesting is the fact that no one configuration provides the best conversion at all Reynolds numbers. Figure 21 is a bar graph of the conversion levels reached by the two triangle configurations at  $Re = 1$ .

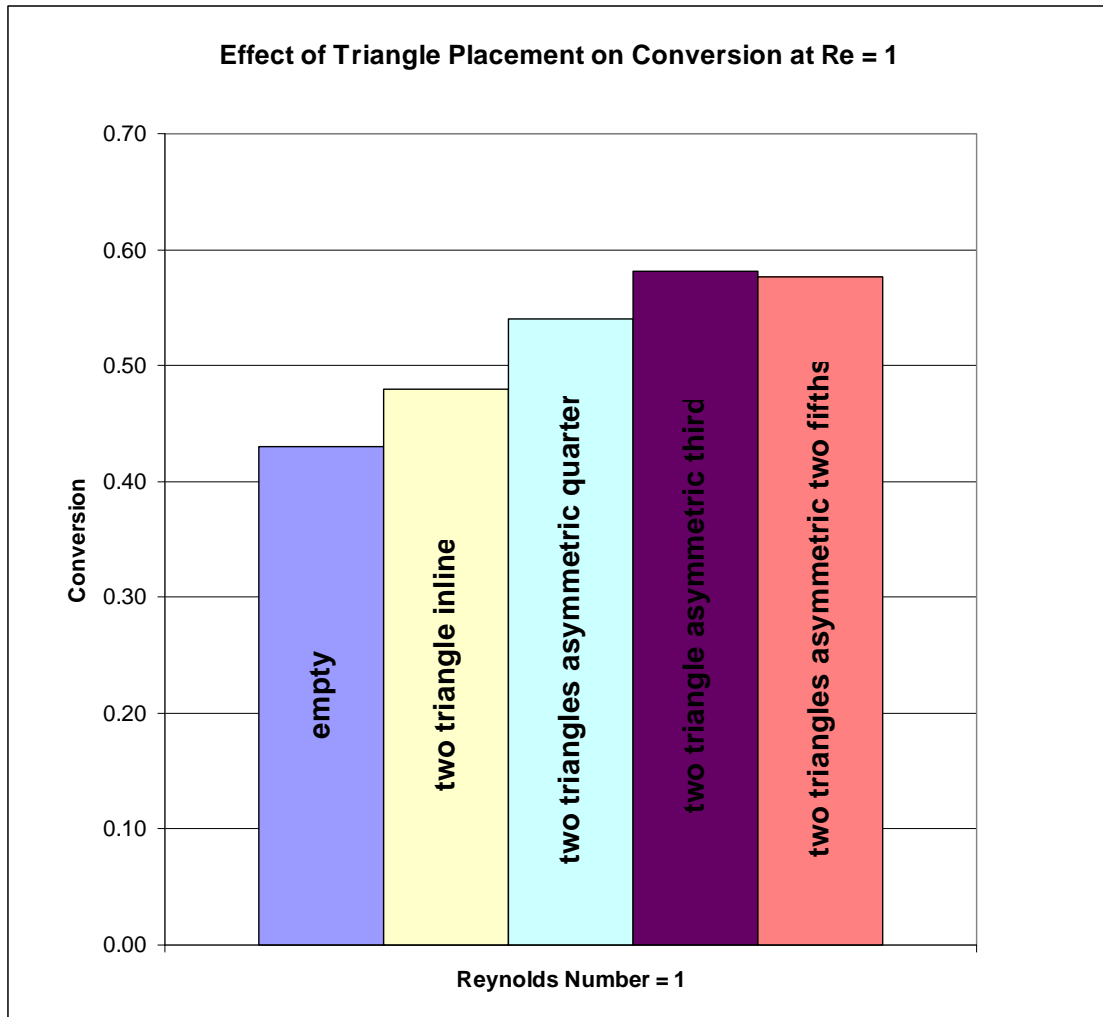


**Figure 21. Comparison of the Effect of Two Triangle Placement on Conversion at Re=1**

At a  $Re = 1$ , the  $1/3$  and  $2/5$  configurations give similar conversion levels of 58.2% and 57.6% respectively. It can be seen in the related flow fields (Figure 18 and Figure 17) that the  $1/3$  configuration produces a higher fluid velocity and hence more flow between the two triangles, achieving slightly better cross-channel fluid redistribution. The  $1/4$  and inline configurations give lower conversion levels, 54.0% and 48.0% respectively. Their respective flow fields (Figure 11 and Figure 13) show

less fluid redistribution to the walls than the 1/3 and 2/5 configurations. Figure 22 is a bar graph of the conversion levels reached by the two triangle configurations at  $Re = 10$ .

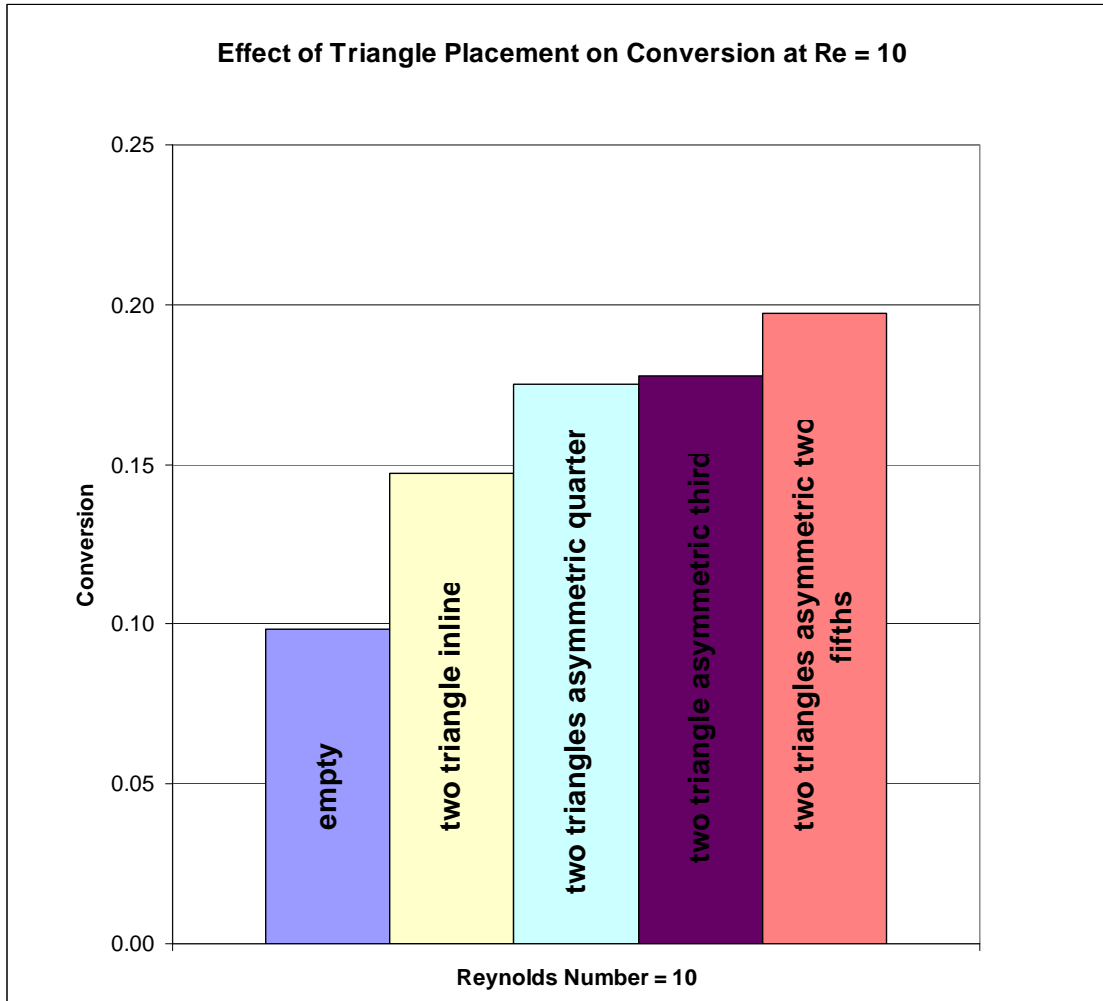


**Figure 22. Comparison of the Effect of Two Triangle Placement on Conversion at  $Re=10$**

As the flow rate increases, the optimal triangle position changes. Here, the 2/5 configuration proves most effective with a conversion of 19.8%, which is approximately double that of the empty channel. Also, simply by changing the

position of the triangles, the conversion may be improved by 33% (2/5 versus Inline). The respective flow field (Figure 17) shows the faster fluid flows occur near the large surface area of the reactive side walls and have a curved shape, indicating angled fluid velocities. The 1/3 configuration and 1/4 configuration produce slightly lower levels of conversion, giving 17.8% and 17.5% conversion respectively. Although their respective flow fields (Figure 18 and Figure 13) show serpentine shaped flows, the concentration of high velocity fluid in the center and away from the reactive side walls is the cause of their lower conversions. The inline configuration gives an even lower conversion of 14.7% due to its even more uneven flow distribution (Figure 11). Here, the fastest fluid velocities are directed straight down the channel with hardly any angled flows. Also, the merging of the triangles' wake regions prevent any cross-channel fluid redistribution and reduce the fluid contact with the enzyme active triangle sides.

At a  $Re = 100$ , the conversion levels are minimal (bar graph in Appendix, Figure A5). The 1/3 and 1/4 configurations give 4.2% and 4.1% respectively, and the 2/5 and inline configurations both give 3.3%.

### **The Effect of Design on Pressure Drop**

The pressure drops of all cases have been calculated by CFD-ACE + and are shown in Figure 23. Higher packing populations cause significantly higher pressure drops at all Reynolds numbers. This is due to the increased drag of greater surface area and the more complex flow fields caused by the additional packing.

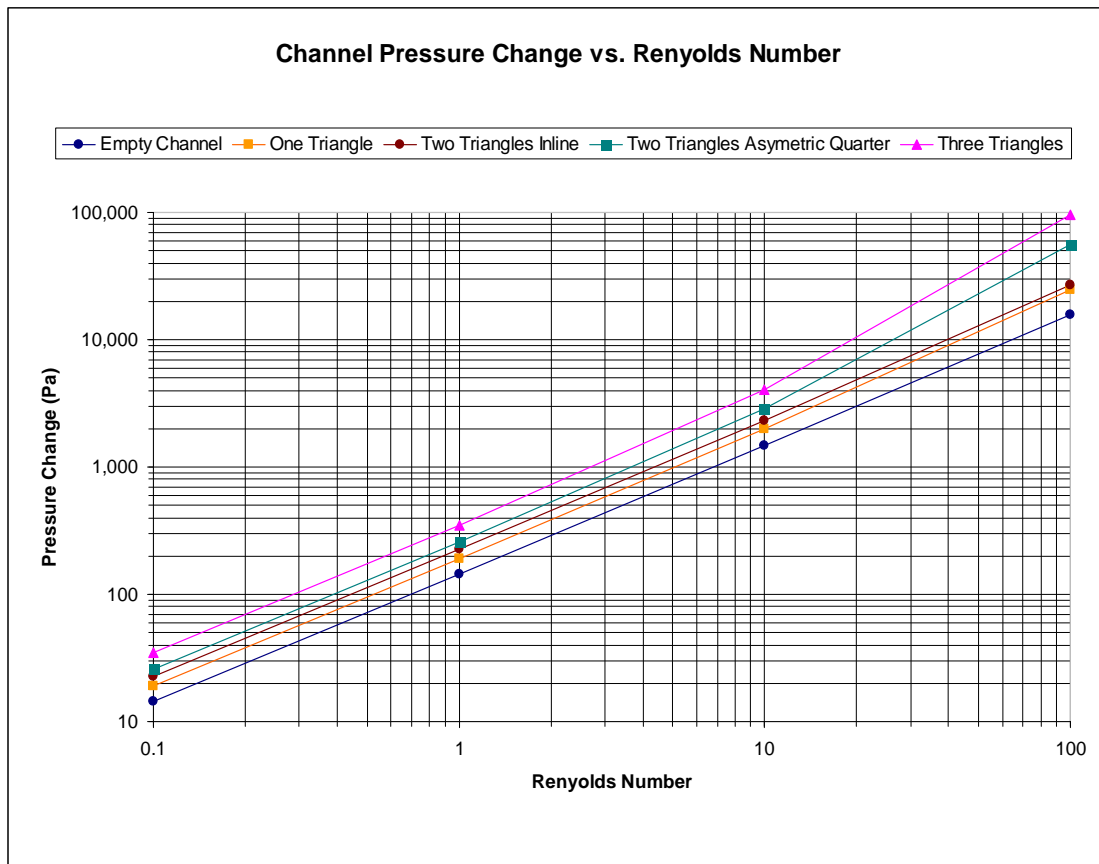


**Figure 23. The Effect of Channel Design on Pressure Drop Through Microchannels**

From  $Re = 0.1$  to  $Re = 10$ , the pressure drop increases in a consistent pattern for all configurations. This steadiness changes between  $Re=10$  and  $Re=100$  for all configurations. This is due to significant flow field changes that occur in this range as shown previously for each configuration (for example, Figure 14). Since pressure drops across any of the two triangle channels follow a similar pattern as illustrated above, they are not discussed here. Their respective pressure drop graph is included in the Appendix (Figure A6).

A pressure drop of 100,000 Pa is not experimentally problematic; that is, it would not present problems to the physical equipment previously tested. However,

since pressure drop is proportional to the length of the channel, a reactor channel significantly longer than the present channel of 10mm may fail structurally or at the seals. Reactors as long as 50cm have been used in the past. Therefore, pressure drop is a constraint on design.

### **Effect of Design on Shear Stress at the Walls**

The shearing force that a flowing fluid imposes along a wall increases with the velocity of the fluid as discussed in the Theory section. For a bioreactor, the forces along the walls may affect immobilized enzymes. Two modes of enzyme related failure could occur under high shear conditions and compromise the effectiveness of the bioreactor: (1) the enzymes and their attachment matrix may become dislodged due to high shear stresses and exit with the flowing fluid, or (2) high shear stresses may essentially inhibit the function of or even destroy enzymes [9]. For example, in studies of a bioartificial liver reactor, shear stresses greater than  $5 \text{ dyne/cm}^2$  were found to diminish the function of hepatocyte cells attached to the reactor floor [11]. Since enzymes have not been tested in this sense,  $5 \text{ dyne/cm}^2$  is taken as a heuristic for this study. The shear stresses resulting at the walls of the various configurations simulated are presented in Table 4.

**Table 4. Effect of Design on Shear Stress at Walls**

Channel Type	Reynolds number	Shear Stress at Walls (dyne/cm <sup>2</sup> )
empty	0.1	0.009
	1	0.090
	10	0.91
	100	9.8
1 triangle	0.1	0.011
	1	0.108
	10	1.13
	100	14.2
2 triangle inline	0.1	0.013
	1	0.128
	10	1.32
	100	15.3
2 triangle asymmetric quarter	0.1	0.015
	1	0.147
	10	1.64
	100	31.8
3 triangle	0.1	0.020
	1	0.199
	10	2.30
	100	55.0

In this reactor, all wall shear stresses at  $Re = 100$  are in the damaging range.

Therefore, a physical microreactor may not perform as predicted by the model at this  $Re$  due to enzyme sensitivity to forces that was not accounted for.

## Conclusions

In all cases, the addition of triangular packing particles increases conversion compared to empty channels. These increases are always greater than the increase in reactive surface area. In fact, conversion has been increased by as much as 150%. Increased conversion is directly attributable to redirecting flow toward reactive surfaces.

Changing packing position changes flow patterns and the amount of mixing. Conversion has been improved by as much as 35% due to varying the packing positions in a two triangle per unit cell system.

Pressure drop increases with packing population and fluid velocity. Pressure drops may become problematic at Reynolds numbers above 10 for more heavily packed channels. Higher pressures may threaten the structural integrity of actual microdevices.

The shear stresses at surfaces due to Reynolds numbers of 10 or greater may threaten the functions of the enzymes or cells attached to the walls of actual microdevices. Future studies may explore these effects further in physical experimentation.

These findings are directly applicable to current microreactor research in the areas of biodiesel, bioartificial organs, and pharmaceuticals. Since packed microchannels have been minimally investigated up to this point, the results of this study may improve the efficiency of existing microreactors. This may also make microprocessing an option for previously overlooked processes that require ample mixing of the entering fluid or fluids.

Future computational research for the optimization of microreactors is recommended. This should include the use of various packing shapes and further investigation of packing placement. A study of micromixing in terms of mixing length would also be revealing. Also, physical experimentation to understand the accuracy of the model predictions is recommended.

## References

1. Jones, F., Forrest, S., Palmer, J., Lu, Z., Elmore, J., and Elmore, B. (2004), *Applied Biochemistry and Biotechnology*. Vol. 113-116, Pg. 261-272.
2. Jones, F., Lu, Z., and Elmore, B. (2002), *Applied Biochemistry and Biotechnology*. Vol. 98-100, Pg. 627-640.
3. Baily, R., Jones, F., Fisher, B., and Elmore, B. (2005), *Applied Biochemistry and Biotechnology*. Vol. 121-124, Pg. 639-652.
4. CFD Research Corporation. (2003), *CFD-ACE(U) User's Manual*, Huntsville, AL.
5. Jones, F., Bailey, R., Wilson, S., and Hiestand, J. (2006), *The Effects of Engineering Design on Heterogeneous Biocatalysis in Microchannels*. (In submission) *Applied Biochemistry and Biotechnology*
6. Laidler, K. J. and Hoare, J. P. J. (1950), *American Chemical Society*. Vol. 72, Pg. 2487-2494.
7. Grubhofer, N. and Schleith, L. (1954), *Z. Physiol. Chem.* Vol. 297, Pg. 108.
8. Madou, M. (1997), *Fundamentals of Microfabrication*, CRC Press, NY.
9. Jones, F., Wen, J., and Elmore, B. (2006), *Enzyme Immobilization using Layer-by-Layer Self-Assembly in PDMS Biomicroreactors*. (In submission) *Applied Biochemistry and Biotechnology*
10. Decher, G., "Fuzzy Nanoassemblies: Toward Layered Polymeric Multicomposites", *Science* 1997, 227, 1232-1237.
11. Park, J., Berthiaume, F., Toner, M., Yarmush, M., and Tilles, A. *Microfabricated Grooved Substrates as Platforms for Bioartificial Liver Reactors*. Published online: <http://www.interscience.wiley.com>. 15 April 2005.
12. Van Doormaal, J. and Raithby, G. (1984), *Numer. Heat Transfer* **7**, 147–163

13. Crowe, C., Roberson, J., and Elger, D. (2001), *Engineering Fluid Mechanics*, 7<sup>th</sup> ed., John Wiley & Sons, New York.
14. DeTurck, D., Gladney, L., and Pietrovito, A. (1996), *The Interactive Textbook of PFP 96*,  
[http://dept.physics.upenn.edu/courses/gladney/mathphys/subsection4\\_1\\_7.html](http://dept.physics.upenn.edu/courses/gladney/mathphys/subsection4_1_7.html), University of Pennsylvania, Philadelphia.

## Appendix

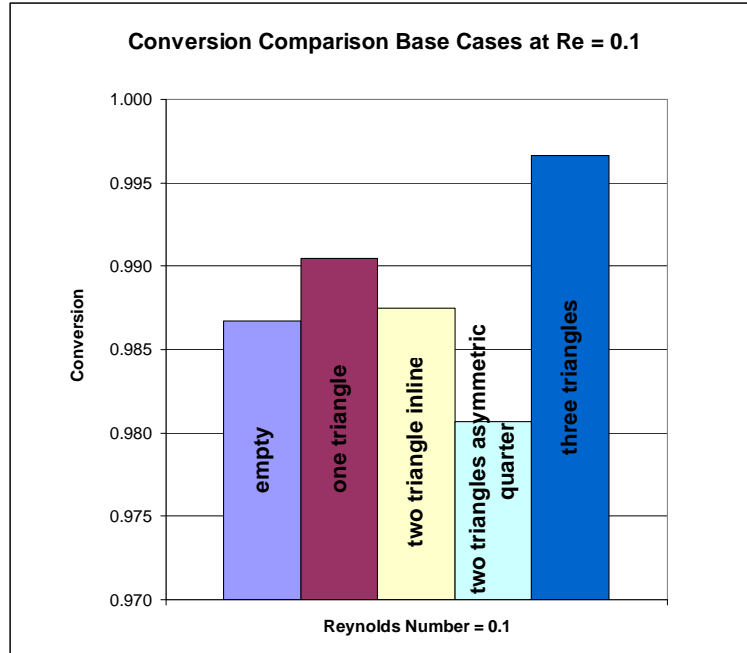


Figure A1. Comparison of the Effect of Packing Configuration on Conversion at Re=0.1

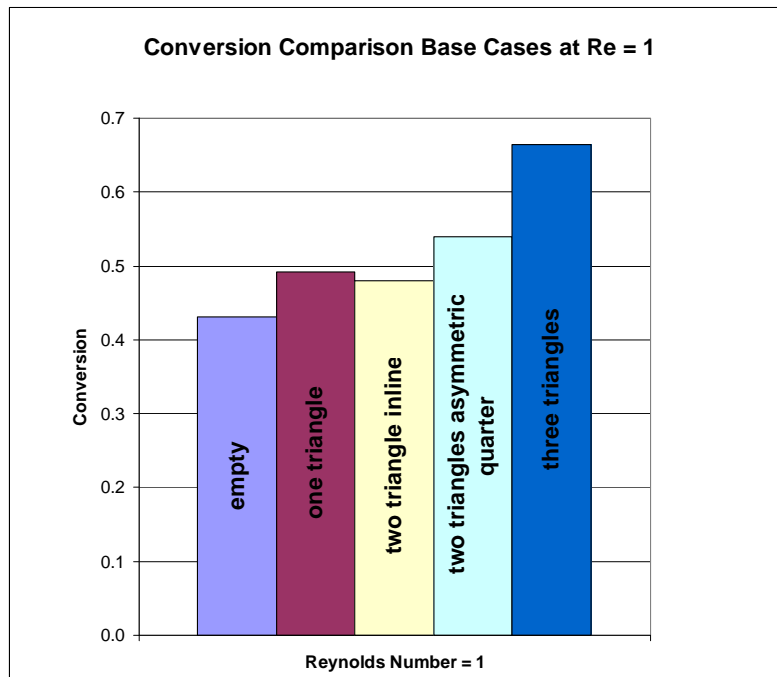


Figure A2. Comparison of the Effect of Packing Configuration on Conversion at Re=1

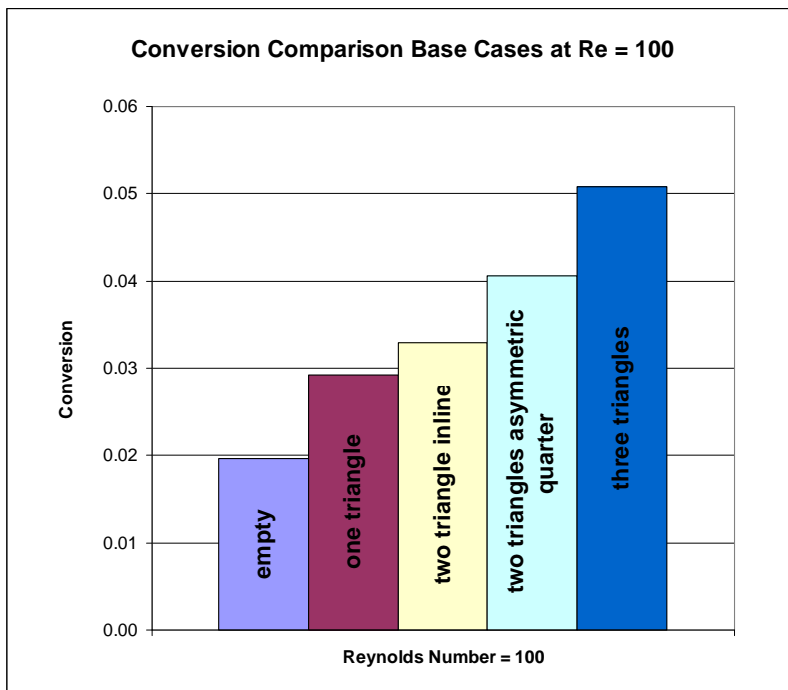


Figure A3. Comparison of the Effect of Packing Configuration on Conversion at Re=100

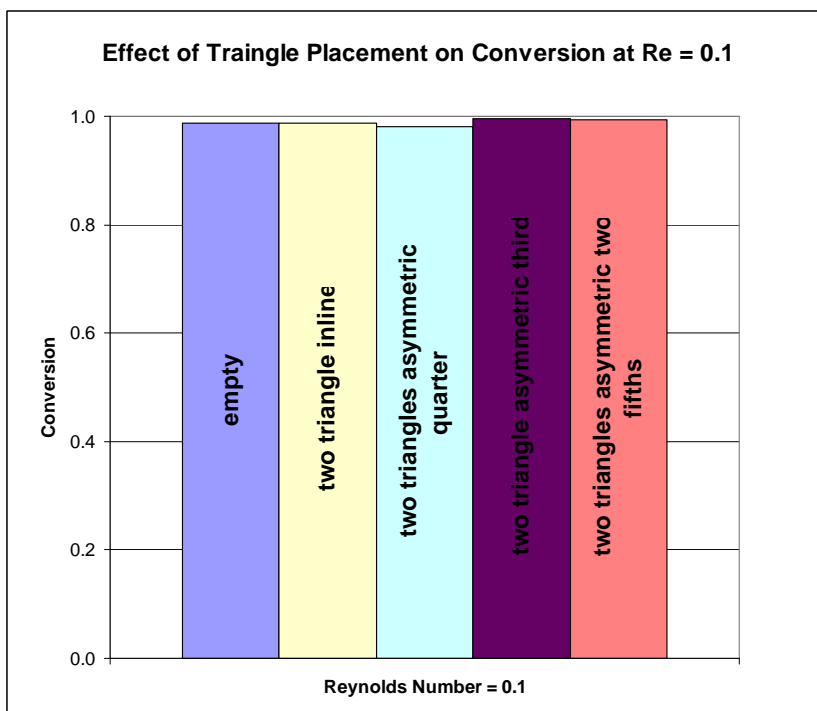


Figure A4. Comparison of the Effect of Two Triangle Placement on Conversion at Re=0.1

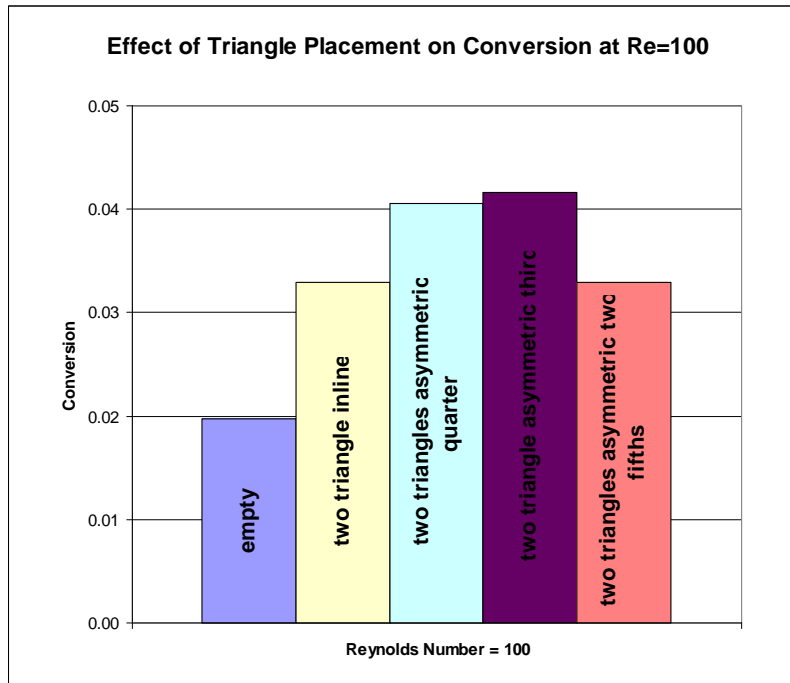


Figure A5. Comparison of the Effect of Two Triangle Placement on Conversion at Re=100

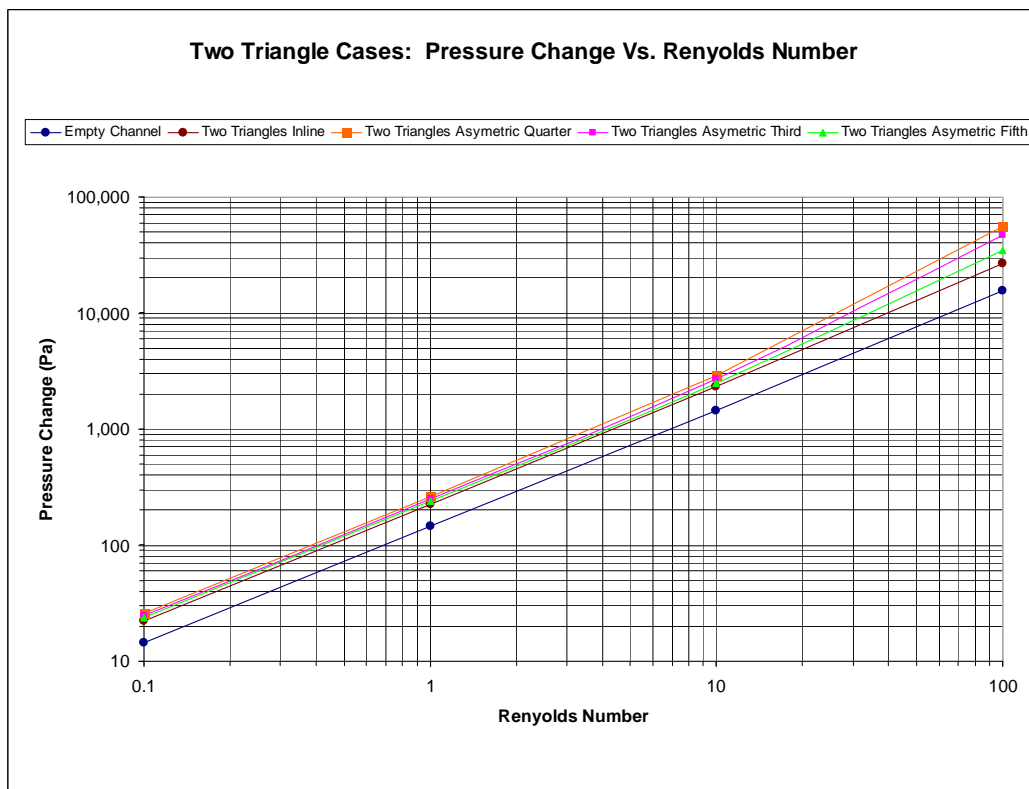


Figure A6. The Effect of Packing Location on Pressure Drop Through Microchannels